AMERICAN SOCIETY FOR MICROBIOLOGY | Antimicrobial Agents and Chemotherapy®

ANTIVIRAL AGENTS

Orally Efficacious Broad-Spectrum Ribonucleoside Analog Inhibitor of Influenza and Respiratory Syncytial Viruses

Jeong-Joong Yoon,[a] Mart Toots,[a] Sujin Lee,[b,c] Myung-Eun Lee,[a] Barbara Ludeke,[d] Jasmina M. Luczo,[e] Ketaki Ganti,[f] Robert M. Cox,[a] Zachary M. Sticher,[g] Vindya Edpuganti,[g] Deborah G. Mitchell,[g] Mark A. Lockwood,[g] Alexander A. Kolykhalov,[g] Alexander L. Greninger,[h] Martin L. Moore,[b,c] George R. Painter,[g] Anice C. Lowen,[f] Stephen M. Tompkins,[e] Rachel Fearns,[d] Michael G. Natchus,[g] Richard K. Plemper[a]

[a]Institute for Biomedical Sciences, Georgia State University, Atlanta, Georgia, USA
[b]Department of Pediatrics, Emory University School of Medicine, Atlanta, Georgia, USA
[c]Children's Healthcare of Atlanta, Atlanta, Georgia, USA
[d]Department of Microbiology, Boston University School of Medicine, Boston, Massachusetts, USA
[e]Center for Vaccines and Immunology, University of Georgia, Athens, Georgia, USA
[f]Department of Microbiology and Immunology, Emory University School of Medicine, Atlanta, Georgia, USA
[g]Emory Institute for Drug Development, Emory University, Atlanta, Georgia, USA
[h]Virology Division, Department of Laboratory Medicine, University of Washington, Seattle, Washington, USA

ABSTRACT Morbidity and mortality resulting from influenza-like disease are a threat, especially for older adults. To improve case management, next-generation broad-spectrum antiviral therapeutics that are efficacious against major drivers of influenza-like disease, including influenza viruses and respiratory syncytial virus (RSV), are urgently needed. Using a dual-pathogen high-throughput screening protocol for influenza A virus (IAV) and RSV inhibitors, we have identified N^4-hydroxycytidine (NHC) as a potent inhibitor of RSV, influenza B viruses, and IAVs of human, avian, and swine origins. Biochemical *in vitro* polymerase assays and viral RNA sequencing revealed that the ribonucleotide analog is incorporated into nascent viral RNAs in place of cytidine, increasing the frequency of viral mutagenesis. Viral passaging in cell culture in the presence of an inhibitor did not induce robust resistance. Pharmacokinetic profiling demonstrated dose-dependent oral bioavailability of 36 to 56%, sustained levels of the active 5′-triphosphate anabolite in primary human airway cells and mouse lung tissue, and good tolerability after extended dosing at 800 mg/kg of body weight/day. The compound was orally efficacious against RSV and both seasonal and highly pathogenic avian IAVs in mouse models, reducing lung virus loads and alleviating disease biomarkers. Oral dosing reduced IAV burdens in a guinea pig transmission model and suppressed virus spread to uninfected contact animals through direct transmission. Based on its broad-spectrum efficacy and pharmacokinetic properties, NHC is a promising candidate for future clinical development as a treatment option for influenza-like diseases.

KEYWORDS antiviral agents, influenza, nucleoside analogs, respiratory syncytial virus

The clinical burden of respiratory viruses associated with influenza-like diseases is highest for the elderly, the immunocompromised, and the very young. Patients above 65 years of age, for instance, are most heavily affected by seasonal influenza, followed by infants (1). Although an inverse patient age group distribution is seen for respiratory syncytial virus (RSV), a member of the *Pneumoviridae* family, the substantial threat caused by severe RSV disease to the elderly is increasingly appreciated (2), and case fatalities associated with both influenza virus and RSV infections disproportionally affect older adults (3). Amplifying the need for next-generation antiviral therapeutics for improved management of respiratory virus infections, the effectiveness of the current

Received 16 April 2018 **Returned for modification** 16 May 2018 **Accepted** 31 May 2018

Accepted manuscript posted online 11 June 2018

Citation Yoon J-J, Toots M, Lee S, Lee M-E, Ludeke B, Luczo JM, Ganti K, Cox RM, Sticher ZM, Edpuganti V, Mitchell DG, Lockwood MA, Kolykhalov AA, Greninger AL, Moore ML, Painter GR, Lowen AC, Tompkins SM, Fearns R, Natchus MG, Plemper RK. 2018. Orally efficacious broad-spectrum ribonucleoside analog inhibitor of influenza and respiratory syncytial viruses. Antimicrob Agents Chemother 62:e00766-18. https://doi.org/10.1128/AAC.00766-18.

Address correspondence to Richard K. Plemper, rplemper@gsu.edu.

J.-J.Y. and M.T. contributed equally to the study.

tri- or quadrivalent influenza vaccine is limited to approximately 60% in adults and only 40% in the elderly, even under the best circumstances (4). However, substantially lower vaccine efficacy has been seen, for instance, in the particularly severe 2017-2018 influenza season (5). No active vaccination is currently available to protect against RSV infection. Passive monoclonal antibody immunoprophylaxis can be administered to high-risk patients, but an estimated $300,000 cost to prevent a single RSV hospitalization (6–11, 83) is prohibitive to broad application.

Since seasonal influenza and RSV outbreaks overlap in temperate regions, clinical symptoms are often nonspecific, and laboratory typing is often not routine outside clinical centers and/or hampered by cost constraints (1), an umbrella diagnosis of influenza-like disease with an unclear nature of the etiologic agent remains common. This ambiguous diagnosis compromises the efficacy of antiviral agents with anticipated narrow therapeutic windows (12–14). We therefore propose that next-generation therapeutics with a broad antiviral indication spectrum, including, as a minimum, influenza viruses and RSV, will be required to improve the management of influenza-like disease.

Generating truly broad-spectrum inhibitors has been a long-coveted goal of antiviral drug development. Discovery efforts have concentrated mainly on two areas: (i) host-targeted antivirals that are immunomodulatory or interfere with cellular factors required for successful virus replication and (ii) direct-acting inhibitors targeting a druggable site or activity conserved across different viral families.

Therapeutic targeting of host factors recruited for virus replication has attracted renewed interest in the past decade due to the combined promise of expanding the antiviral indication range and reducing the frequency of viral escape from inhibition (15–18). Although host-directed candidates have largely met these expectations in experimental settings (15, 16), the approach has yet to deliver approved therapeutics with safety profiles acceptable for human use against viral diseases such as seasonal influenza and RSV disease (19). Direct-targeted antivirals typically display more-promising initial toxicity profiles, but the quest for broad-spectrum inhibitory activity has fueled the rediscovery of many promiscuous, often covalently reactive scaffolds that are associated with unclear mechanisms of activity (20–23). Based on their demonstrated history of ultimate failure in development, many of these scaffolds are considered undesirable and were classified as frequently hitting pan-assay interfering (PAIN) substances (21, 24). As a notable exception, different ribonucleoside analogs have been identified, which combine good clinical promise with a broadened indication spectrum, often showing a remarkable preference for a range of viral over host cell polymerases.

While no nucleoside analog inhibitor is currently in clinical use against influenza viruses in the United States, the allosteric endonuclease blocker baloxavir marboxil (xofluza) was recently approved for sale in Japan. Furthermore, ribavirin is licensed for the treatment of RSV infection, and T-705 (favipiravir) is conditionally approved for stockpiling in Japan in a situation where a pandemic is caused by oseltamivir-resistant influenza virus. However, toxicity liabilities and limited efficacy undermine the clinical use of ribavirin (25, 26), and the potential for teratogenicity (27) may compromise the use of T-705 for the treatment of influenza. The ribonucleoside analog ALS-8176 was found to be efficacious in a human RSV challenge study (28), providing an important proof of concept for the treatment of influenza-like diseases with competitive polymerase inhibitors, but ALS-8176 did not inhibit influenza virus (29).

Toward the ultimate goal of identifying developable broad-spectrum medications against influenza-like disease, we have established and validated a replication-competent dual RSV and influenza A virus (IAV) reporter virus-based high-throughput screening (HTS) assay that allows the simultaneous identification of IAV-specific, RSV-specific, and dually active, potentially broad-spectrum, hit candidates (30). The first implementation of this protocol against a large open discovery library of small-molecule compounds has yielded promising target-specific inhibitors of RSV (31) and influenza virus (32), but broad-spectrum hits remained limited to undesirable scaffolds and clinically undevelopable compounds interfering with pyrimidine *de novo* synthesis

(32–34). In this study, we applied the assay to a collection of ribonucleoside analogs. Having identified a cytidine analog with potent activity against both target viruses, we initiated mechanistic characterization of RSV and IAV RNA-dependent RNA polymerase (RdRp) inhibition; evaluated potency against a panel of laboratory-adapted and clinical strains representing RSV, IAVs, and influenza B viruses (IBVs) in established cell lines and primary human bronchial tracheal epithelial cells (HBTECs); determined oral pharmacokinetic profiles in the murine respiratory tract; assessed potency against RSV and both seasonal and highly pathogenic IAV subtypes in mouse models; and examined the effect of treatment on influenza virus spread in the guinea pig IAV transmission model. Collectively, these assays identify the compound as an orally efficacious broad-spectrum inhibitor of influenza-like disease caused by RSV or influenza virus infections.

RESULTS

Having assembled an in-house library of 102 ribonucleoside analog candidates, we sampled the set in three replicates using our validated dual-pathogen HTS protocol (30). This campaign yielded three hit candidates that consistently blocked both viral targets in the primary assay and, in addition, two RSV-specific and one influenza virus-specific candidate (Fig. 1A).

Indication spectrum of a dually active HTS hit candidate. Focusing on the dual-active compounds only, two candidates were excluded based on excessive toxicity in dose-response potency and toxicity counterscreens (see Fig. S1 in the supplemental material), while the remaining candidate (dual 1, EIDD-1931 or N^4-hydroxycytidine [NHC]) (Fig. 1B) showed active concentrations in the nanomolar to low-micromolar range and selectivity indices (SIs) (SI = CC_{50} [50% cytotoxic concentration]/EC_{50} [50% effective concentration]) of ≥89 against a broad panel of RSV, IAV, and IBV laboratory strains and isolates (Table 1). This group included clinical RSV isolates cultured from nasal wash specimens (Fig. 1C); IAVs of human, avian, and swine origins representing both group 1 and 2 hemagglutinins (HAs) (Fig. 1D and Table 1); highly pathogenic H5N1 and emerging H7N9 avian IAVs (AIVs) (Fig. 1E); and IBVs representing both circulating lineages (35), Victoria and Yamagata (Fig. 1F). A subset of avian influenza viruses was tested *in ovo* (Table 1), demonstrating NHC potency in primary cells. Consistent with the high initial SI values in cultured cells, embryo development in the treated chicken eggs was visually unaffected by the compound (Fig. S2). Whereas T-705 was inactive in primary HBTECs, the antiviral activity of NHC against both RSV and influenza virus was unchanged in these disease-relevant human primary cells compared to immortalized cell lines (Fig. 1G). Drug combination testing of NHC and the current standard of care (SOC) against IAV infection, oseltamivir, in cultured cells identified an extended plateau area of medium-level antiviral synergy (HSA model), while no significant increase in cytotoxicity was noted in the presence of the drug combination (Fig. S3). These data demonstrate the activity of NHC against a panel of respiratory viruses associated with influenza-like diseases. Combined with the previously reported antiviral activity of NHC in cell culture against some *Flaviviridae*, *Coronaviridae*, and *Togaviridae* family members (36–39), these data establish the broad-spectrum activity of the compound against different positive- and negative-strand RNA virus families and, in the case of IAV infection, spotlight the potential for synergistic combination with the current SOC.

Mechanistic assessment of NHC. Based on the reversal of NHC-mediated inhibition of a chikungunya virus replicon through an excess of exogenous cytidine and uridine, the compound was thought to behave as a pyrimidine analog *in cellula* (37). We first confirmed through time-of-addition variation studies that NHC blocks a postentry step in the influenza virus and RSV replication cycles (Fig. 2A). Plasmid-based minigenome reporter assays validated in both cases NHC interference with viral RdRp activity (Fig. 2B). However, an *in vitro* activity assay using host cell polymerase α did not reveal inhibition of the cellular polymerase by the active 5′-triphosphate form of the compound, NHC-TP (Fig. 2C). As previously observed for positive-strand RNA virus replicons, the inhibition of RSV and influenza virus by NHC can be reversed through the addition of exogenous pyrimidines

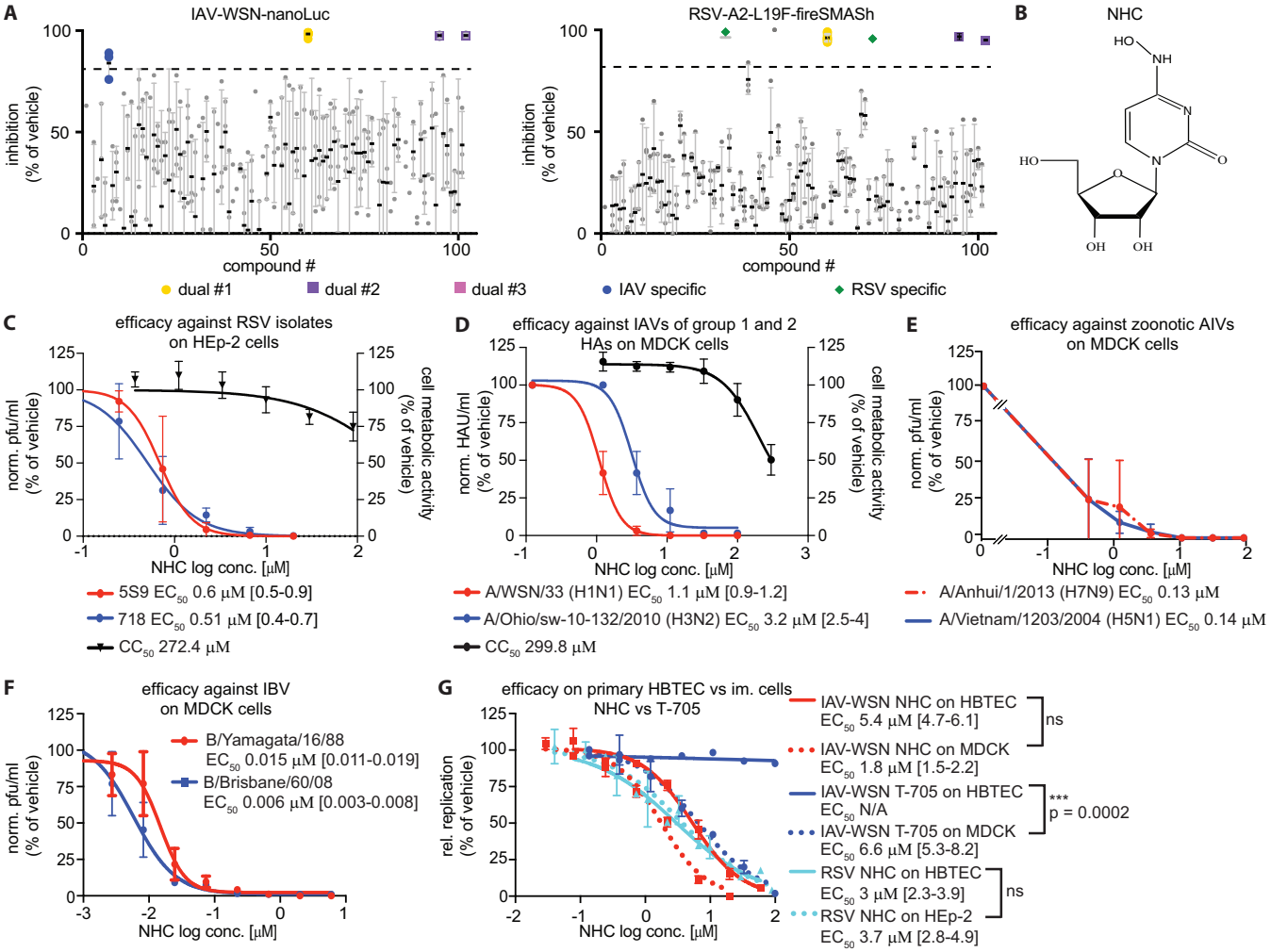

FIG 1 The ribonucleoside analog NHC blocks negative-strand RNA viruses associated with influenza-like diseases. (A) Simultaneous anti-RSV and anti-IAV screen of a ribonucleoside analog library, carried out in triplicate. Shown are individual biological replicates (gray symbols) and mean values (black lines) ± SD. Hit candidates are highlighted in color, with a hit cutoff of ≥80% inhibition. (B) Structure of the NHC hit candidate. (C to G) For all dose-response measurements, symbols represent means ± SD of data from at least three biological repeats, expressed relative to values for vehicle (DMSO)-treated controls. EC_{50} and CC_{50} values were calculated through four-parameter variable-slope regression modeling, with 95% confidence intervals in brackets. (C) NHC activity against two RSV isolates on HEp-2 cells. Virus titration was performed by a plaque assay. PrestoBlue reagent was used to determine the effect of treatment on cell metabolic activity. (D) NHC activity against viruses representing group 1 and 2 HAs on MDCK cells. Virus titration was performed by HA assay and is expressed as relative HA units per milliliter (HAU/ml). (E) Efficacy of NHC against an HPAIV and an emerging AIV subtype on MDCK cells. Virus titration was performed by a plaque assay. (F) Efficacy of NHC against IBVs representing both currently circulating lineages on MDCK cells. Virus titration was performed by $TCID_{50}$ assays. (G) Comparison of NHC and T-705 antiviral efficacies on primary human bronchial tracheal epithelial cells (HBTEC) versus immortalized (im.) MDCK or HEp-2 cells. Virus replication assessment was based on virus-encoded luciferase reporter activity. Analysis was performed by two-way ANOVA, and *P* values are shown (ns, not significant).

but not purines (Fig. 2D). To determine whether NHC-TP is accepted by negative-strand RNA virus RdRps as a substitute for CTP or acts as a chain terminator, we employed a biochemical assay of RSV polymerase activity that uses purified viral phosphoprotein (P) and large protein (L) RSV polymerase components, a nucleoside triphosphate (NTP) mix, and a synthetic oligonucleotide template, resulting in a 23-mer product (40). Without CTP in the NTP mix, polymerization is stalled at the first guanidine residue in the template, releasing 14-mer amplicons. The addition of NHC-TP partially restored the generation of full-length 23-mer amplicons, demonstrating that the RSV RdRp complex accepts NHC in place of cytidine and that the compound does not act as an obligatory chain terminator (Fig. 2E). Rather, we noted significantly increased frequencies of C-to-U, G-to-A, and, in the case of RSV only, A-to-G transition mutations in viral RNA after single-cycle infection of cells in the presence of 10 μM NHC, followed by subcloning of individual viral RNA-derived cDNA amplicons and Sanger sequencing

TABLE 1 NHC efficacy against a panel of influenza virus and RSV isolates[a]

Viral strain	Assay method, host system	EC_{50} (μM) (95% confidence interval)	SI	Origin
A/WSN/33 (H1N1)	Plaque assay, MDCK cells	3.1 (2.25–3.82)	98	Human
A/WSN/33 (H1N1)	$TCID_{50}$-HA assay, MDCK cells	1.1 (0.86–1.22)	275	Human
A/California/7/2009 (H1N1) pdm09	$TCID_{50}$-HA assay, MDCK cells	3.1 (1.49–6.23)	98	Human pdm09
A/Georgia/M5081/2012 (H1N1)	$TCID_{50}$-HA assay, MDCK cells	3.4 (2.92–3.9)	89	Human pdm09
A/Netherlands/602/2009 (H1N1) pdm09	$TCID_{50}$-HA assay, MDCK cells	1.8 (1.17–2.55)	171	Human pdm09
A/duck/Alberta/35/76 (H1N1)	HA assay, *in ovo*	0.6 (0.45–0.48)	NA	Avian
A/swine/Spain/53207/2004 (H1N1)	HA assay, *in ovo*	0.1 (0.02–0.12)	NA	Swine; Eurasian avian-like
A/chicken/Potsdam/178-4/83 (H2N2)	HA assay, *in ovo*	0.4 (0.15–1.35)	NA	Avian
A/Vietnam/1203/2004 (H5N1)	$TCID_{50}$, MDCK cells	0.14	2,143	Avian
A/Anhui/1/2013 (H7N9)	$TCID_{50}$, MDCK cells	0.13	2,308	Avian
A/Aichi/2/68 (H3N2)	$TCID_{50}$-HA assay, MDCK cells	3.2 (2.68–3.88)	93	Human
A/Wisconsin/67/2005 (H3N2)	$TCID_{50}$-HA assay, MDCK cells	1.7 (1.27–2.33)	182	Human
A/Panama/2007/99 (H3N2)	$TCID_{50}$-HA assay, MDCK cells	1.2 (0.05–2.0)	250	Human
A/swine/Ohio/sw10-132/2010 (H3N2)	$TCID_{50}$-HA assay, MDCK cells	3.2 (2.52–4.05)	95	Swine; triple-reassortant lineage
B/Yamagata/16/88	$TCID_{50}$, MDCK cells	0.015 (0.011–0.019)	20,000	Human
B/Brisbane/60/08	$TCID_{50}$, MDCK cells	0.006 (0.003–0.008)	50,000	Human
recRSV-A2-L19F	Reporter assay, HEp-2 cells	3.7 (2.8–4.9)	74	Human
RSV clinical strain 5S9	Plaque assay, HEp-2 cells	0.69 (0.5–0.9)	394	Human
RSV clinical strain 718	Plaque assay, HEp-2 cells	0.51 (0.4–0.7)	533	Human

[a]The potency of NHC against different IAVs, IBVs, and RSVs was determined in cultured cells or embryonated chicken eggs. IAVs are sorted by lineage and subtype. EC_{50}s were determined through four-parameter variable-slope regression modeling, with 95% confidence intervals in parentheses. NA, not applicable.

(Fig. 2F). Relative mutation frequencies were increased approximately 7- to 10-fold (Table 2), but no specific mutation hot spots were detected in the fragment analyzed. This observation is consistent with the postulated ability of NHC to base pair as either cytosine or uracil (41), which may drive the replicating viruses into error catastrophe (36, 42).

Previous attempts to induce robust resistance of two positive-strand RNA viruses, Venezuelan equine encephalitis virus (VEEV) and bovine viral diarrhea virus, from inhibition by NHC were unsuccessful (36, 43). To resistance profile negative-strand RNA virus-derived RdRps, we incubated RSV-A2 and IAV-WSN in the presence of gradually increasing NHC concentrations for 10 consecutive passages. However, no robust resistance (>5-fold increase in EC_{50}s) emerged, indicating a universally high barrier against viral escape from NHC, independent of the target virus examined.

Pharmacokinetics. In preparation for *in vivo* testing, we determined anabolic, pharmacokinetic (PK), and pharmacodynamic (PD) profiles and lung tissue distributions of the compound in primary HBTECs and mice. Liquid chromatography-tandem mass spectrometry (LC-MS/MS) analysis after exposure of HBTECs to 20 μM NHC demonstrated effective conversion to active NHC-TP, represented by a concentration plateau at approximately 4 nmol/10^6 cell over the 24-h time period examined. In contrast, steady-state levels of free prodrug and NHC–5′-monophosphate (NHC-MP) remained flat at a low ~2 pmol/10^6 cells in this period (Fig. 3A). Subsequent washout revealed a high metabolic stability of NHC-TP in the HBTECs, resulting in a calculated half-life exceeding 4 h (Fig. 3B).

For species consistency with our mouse efficacy models of RSV and IAV infection, we determined plasma PK of NHC and lung levels of both NHC and the active antiviral agent NHC-TP in mice. Intraperitoneal (i.p.) and oral (p.o.) administration of different dose levels ranging from 10 to 50 mg/kg of body weight (i.p.) and 50 to 500 mg/kg (p.o.) resulted in dose-dependent increases in overall exposure (area under the concentration-time curve [AUC]) to the prodrug (Fig. 3C) and peak plasma concentrations (C_{max}) after oral dosing exceeding 40 μM (Fig. 3D). Exposure levels corresponded to a dose-dependent oral bioavailability of 36 to 56% (Table 3). The dose dependency of overall prodrug exposure extended to respiratory tissue (Fig. 3E), but peak NHC-TP concentrations in lung saturated above oral dose levels of approximately 150 mg/kg (Fig. 3F). While this C_{max} plateau suggests an anabolism bottleneck of NHC in mouse

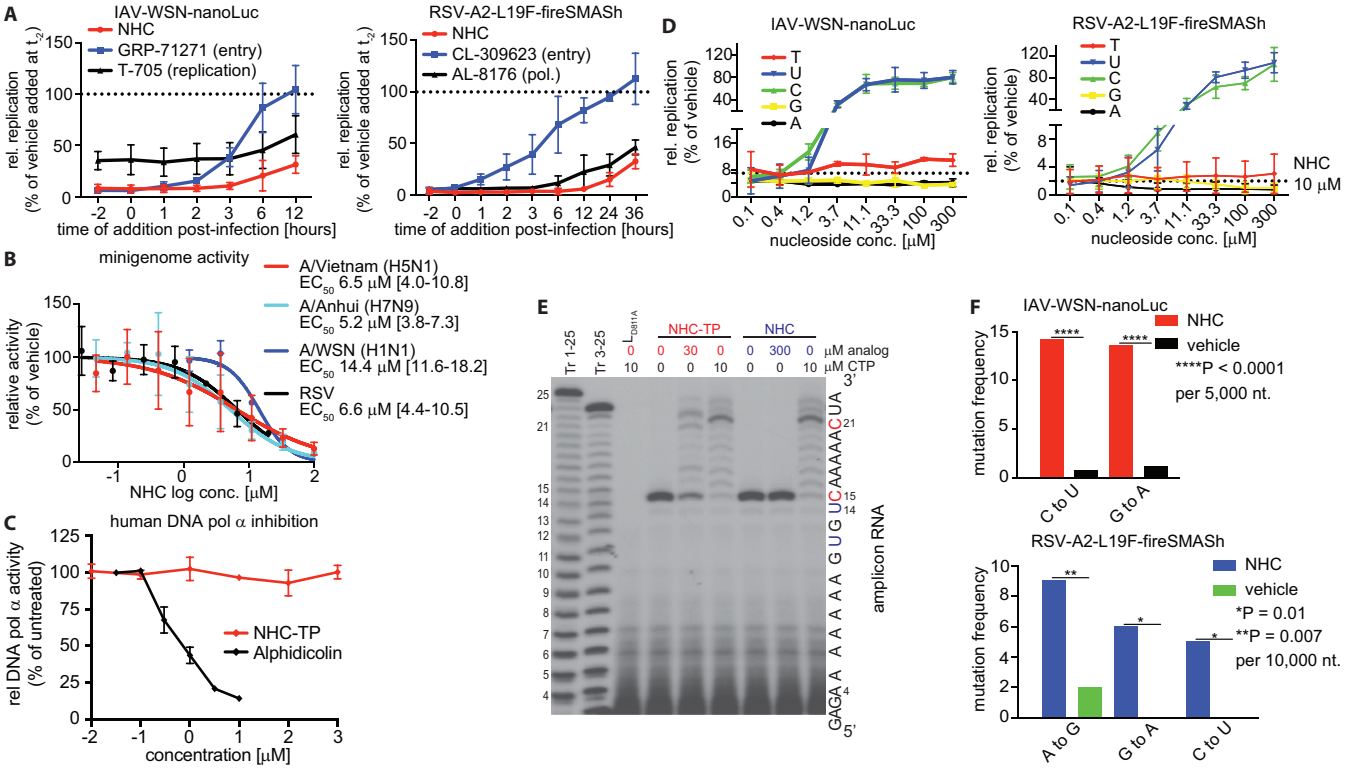

FIG 2 Mechanistic assessment of NHC. (A) Time-of-addition variation assays. (Left) MDCK cells were infected with IAV-WSN-nanoLuc and treated with 10 μM NHC, 50 μM T-705 (positive-control influenza virus RdRp inhibitor) (57), or 10 μM GRP-71271 (positive-control IAV-WSN entry inhibitor) (32) at different times relative to infection. (Right) Hep2 cells were infected with recRSV-A2-L19F-fireSMASh (recombinant RSV) and treated with 10 μM NHC, 10 μM ALS-8176 (positive-control RSV RdRp inhibitor) (29), or 10 μM CL-309623 (positive-control RSV entry inhibitor) (82) at different times relative to infection. Reporter activity is expressed relative to values for vehicle-treated control infections (dashed lines; volume-equivalent DMSO was added to the controls two hours before infection [t_{-2}]). Values represent means of data from three biological repeats ± SD. (B) NHC activity in dose-response minigenome assays. 293T cells were transiently transfected with IAV-WSN (H1N1), A/Vietnam (H5N1), A/Anhui (H7N9), or RSV minigenome systems. Increasing concentrations of NHC were added to the cells immediately after transfection. Luciferase reporter activity was measured after a 30-h exposure and is expressed relative to values for vehicle-treated wells. Means of data from three biological repeats ± SD are shown. Analysis was done by four-parameter variable-slope regression modeling. (C) Effect of NHC-TP on human DNA polymerase α activity. *In vitro* polymerase assays were carried out in the presence of a range of NHC-TP concentrations or aphidicolin for reference. Symbols represent mean values ± SD of data from 3 biological repeats each. (D) *In cellula* nucleoside competition assay. MDCK cells infected with WSN-nanoLuc (left) or RSV-fireSMASh (right) were exposed to 10 μM NHC and increasing concentrations of exogenously added natural nucleosides at the onset of infection. Values were normalized to the values for vehicle-treated controls and show means of data from three biological repeats ± SD. (E) *In vitro* RSV RdRp activity assay. Purified RSV P-L complexes were incubated with a 25-mer RNA oligonucleotide template and rNTPs (ribonucleotide triphosphate; lacking CTP) with an [α-^{32}P]UTP tracer. NHC (blue), NHC-TP (red), or CTP (black) was added at the specified final concentrations. Controls lacked CTP or contained the inactive L_{D811A} mutant. Lengths of the reaction products were determined by using Tr 1-25 and Tr 3-25 (RNA size markers) standards, and the sequence of the predominant 23-mer amplicon originating from major initiation at the +3 position is shown on the right. (F) Transition mutation frequency in viral RNA. Total RNA was extracted from cells infected with WSN (top) or RSV (bottom) in the presence of 10 μM NHC or the vehicle. Treatment was started immediately at the time of infection. PB1- or L-encoding cDNA was subcloned, and at least 10 independent clones each were subjected to Sanger sequencing; at least 7,737 nucleotides were determined per virus and exposure condition. Statistical analysis was performed with Fisher's exact test.

respiratory tissue at higher prodrug levels, lung tissue distribution assessment revealed sustained concentrations of active NHC-TP of approximately 10 nmol/g lung tissue for over 8 h after administration at the 150- and 500-mg/kg levels. These results highlight the strong potential of NHC for clinical use against influenza-like diseases.

***In vivo* efficacy testing against major causes of influenza-like diseases.** Based on the PK/PD profiles, we selected as the starting point for all experiments oral doses of 100 mg/kg (below the NHC-TP lung tissue plateau level) and 400 mg/kg (comfortably within the NHC-TP tissue saturation range) and a twice-daily (b.i.d.) dosing regimen for *in vivo* efficacy testing against RSV and IAV in mice. For testing against RSV, BALB/cJ mice were infected intranasally (i.n.) with 10^5 PFU each of recombinant RSV-A2-L19F, which is based on the A2 strain but contains an F protein derived from RSV isolate line 19 that increases pathogenicity in the mouse model and better reproduces key features of human RSV disease, such as high lung virus loads, extensive mucus production, and pronounced respiratory distress (44). Treatment was initiated 2 h prior to infection and

TABLE 2 Quantitation of transition mutations in NHC-experienced viral RNA[a]

Virus and treatment	Total no. of nt	No. of transition mutations		
		C to U	G to A	A to G
IAV-WSN				
10 μM NHC	7,737	22	21	2
DMSO	12,539	2	3	4
RSV-A2				
10 μM NHC	9,836	5	6	9
DMSO	10,971	0	0	2

[a]Shown is a summary of data from the mutation frequency analysis of viral RNA after a 24-h exposure of IAV-WSN- or RSV-A2-L19F-infected cells to 10 μM NHC. The percent nucleotide (nt) contents of A, T, G, and C residues were 34.4%, 23.3%, 22.4%, and 19.9%, respectively, for IAV-WSN RNA and 37.4%, 33.3%, 14.6%, and 14.6%, respectively, for RSV-A2 RNA.

continued until lung virus titers were determined at 5 days postinfection. At both dose levels, RSV loads were significantly reduced by more than 1 order of magnitude compared to those in vehicle-treated animals (Fig. 4A). However, we did not detect an appreciable difference in progeny titers between the dose groups, presumably reflecting that even at the lower dose used, the NHC-TP concentration in lung tissue approaches saturation levels. Lung histopathology and periodic acid-Schiff (PAS) staining demonstrated complete suppression of excessive mucin production in the 400-mg/kg group and a partial reduction in animals dosed with 100 mg/kg (see Fig. S4 in the supplemental material). Exploratory dosing at 30 and 50 mg/kg failed to significantly lower lung virus loads (Fig. S5), but oral doses of as low as 30 mg/kg were sufficient to completely ameliorate the severe respiratory distress experienced by vehicle-treated animals (Fig. 4B). These results demonstrate the effective inhibition of RSV replication by NHC *in vivo* at higher dose concentrations. The data furthermore suggest that even minimal pharmaceutical interference with RSV replication can translate into major changes in RSV disease markers in the mouse model.

To test NHC efficacy against seasonal influenza viruses, we infected BALB/cJ mice i.n. with 10^3 PFU of mouse-adapted A/Puerto Rico/8/34 (H1N1) (PR8) and assessed lung viral loads at 6 days postinfection as the primary efficacy milestone. In addition, virus-induced hypothermia and selected proinflammatory cytokines were monitored. Based on the experience with anti-RSV efficacy, we focused on the 100- and 400-mg/kg dose levels only for these experiments. After prophylactic dosing as described above, we again observed significant reductions in lung virus loads in NHC- versus vehicle-treated animals (Fig. 4C). All infected animals experienced virus-induced hypothermia, but symptoms were significantly alleviated in mice treated with high-dose NHC (Fig. S6). To put the antiviral impact of NHC in perspective to the SOC, we orally administered NHC (400-mg/kg dose level only in this experiment) or oseltamivir to PR8-infected mice and determined lung virus load profiles for each treatment group (Fig. 4D). Consistent with previous observations (45), oseltamivir delayed viral replication in the first 2 days after infection, but peak lung titers in the oseltamivir group were not significantly different from those in vehicle-treated animals. In contrast, treatment with NHC caused a significant and sustained reduction in the virus load. Reverse transcription-quantitative PCR (RT-qPCR)-based quantitation of the virus-triggered induction of selected proinflammatory cytokines, gamma interferon (IFN-γ) and interleukin-6 (IL-6), revealed a statistically significant decrease in mean induction levels in the 400-mg/kg group (Fig. 4E).

Since PR8 reaches plateau lung titers within 24 h after infection (Fig. 4D), the time window provided by the mouse model to assess the postexposure efficacy of NHC is narrow. To gain first insight into the effect of delayed dosing onset, we initiated treatment at 6 h postinfection, again administering the compounds at the 400-mg/kg dose level only and continuing with a b.i.d. regimen. Lung virus loads were determined at 3 and 6 days postinfection and showed a significant reduction compared to those in vehicle-treated control animals at both time points (Fig. 4F). In keeping with the results

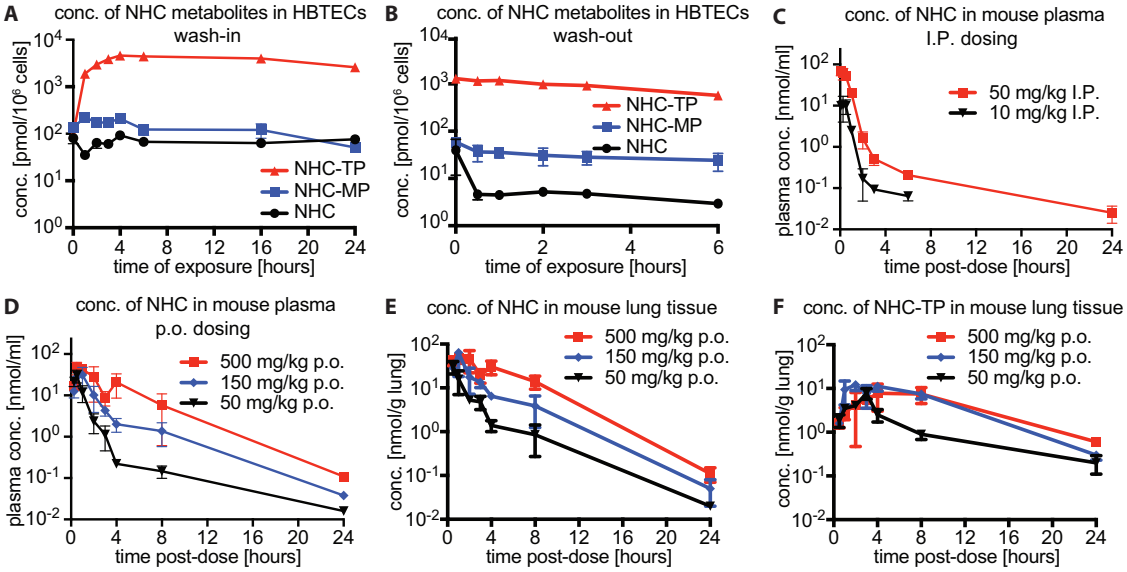

FIG 3 Anabolism and PK/PD profiling of NHC. (A) Anabolism of NHC in primary HBTECs. Cells were incubated with 20 μM NHC for the indicated exposure times, and intracellular concentrations of NHC and anabolites (NHC–5′-monophosphate [NHC-MP] and NHC-TP) were determined by LC-MS/MS. (B) NHC anabolite stability in HBTECs. Cells grown in the presence of 20 μM NHC for 24 h were switched to drug-free medium, and anabolite concentrations were monitored over a 6-h period by LC-MS/MS. (C and D) Time-concentration profiles for plasma levels of NHC after a single i.p. (C) or oral (D) dose in mice (3 animals per time point) at the specified levels. Shown are PK/PD profiles after a single oral dose in mice (3 animals per time point) at the specified levels. (E and F) Lung tissue concentrations of NHC (E) and of the bioactive NHC-TP anabolite (F) after a single oral NHC dose at the specified levels. Samples in panels A to F were analyzed by LC-MS/MS, and symbols represent mean values ± SD of data from 3 biological repeats each.

obtained after prophylactic dosing, virus-induced hypothermia was significantly reduced in the postexposure NHC-treated animals also (Fig. S6), establishing a comparable benefit of NHC for the management of influenza virus infection independent of whether treatment followed a prophylactic or postexposure regimen.

Efficacy against highly pathogenic avian influenza virus and effect on IAV transmission. Having obtained a proof of concept for oral NHC efficacy against PR8 in mice, we employed a highly pathogenic AIV (HPAIV)/mouse model to examine the potential of the compound to strengthen preparedness against highly pathogenic IAVs that constitute a high pandemic threat. Mice were infected i.n. with 6 PFU of A/Vietnam/1203/2004 (H5N1) (A/Vietnam), and treatment was initiated prophylactically at the 400-mg/kg dose level only and continued as described above. Due to the pronounced neuropathogenicity of A/Vietnam in the model (46), both lung and central nervous system (CNS) viral loads were determined at day 6 postinfection in comparison with vehicle- and SOC-treated animals (Fig. 4G). Lung virus titers were again significantly reduced in drug-treated animals compared to the vehicle-only group, and virus was undetectable in the CNS in four out of five animals that had received NHC. This inhibitory effect on A/Vietnam lung virus loads was equivalent to that observed in

TABLE 3 Calculation of PK parameters for NHC after a single i.p. or p.o. dose in mice[a]

Route	Dose (mg/kg)	T_{max} (h)	C_{max} (nmol/ml)	AUC (0–∞) (h · nmol/ml)	V_z-F (liters/kg)	Cl-F (liters/h/kg)	$t_{1/2}$ (h)	Bioavailability (%)
i.p.	10	0.25	10.5	9.8	16	3.9	2.8	NA
i.p.	50	0.08	70.4	62	22.7	3.1	5	NA
p.o.	50	0.5	30.2	31.4	45.8	6.1	5.2	56
p.o.	150	1	31.4	71	37.9	8.2	3.2	43
p.o.	500	0.5	47.2	202.9	36.8	9.5	2.7	36

[a]Parameters and dose-dependent oral bioavailability of NHC were calculated by using the WinNonlin software package (Pharsight). T_{max}, time to maximum concentration of drug in serum; $t_{1/2}$, half-life; V_z-F, apparent volume of distribution during terminal phase after nonintravenous administration; Cl-F, apparent total clearance of the drug from plasma after administration.

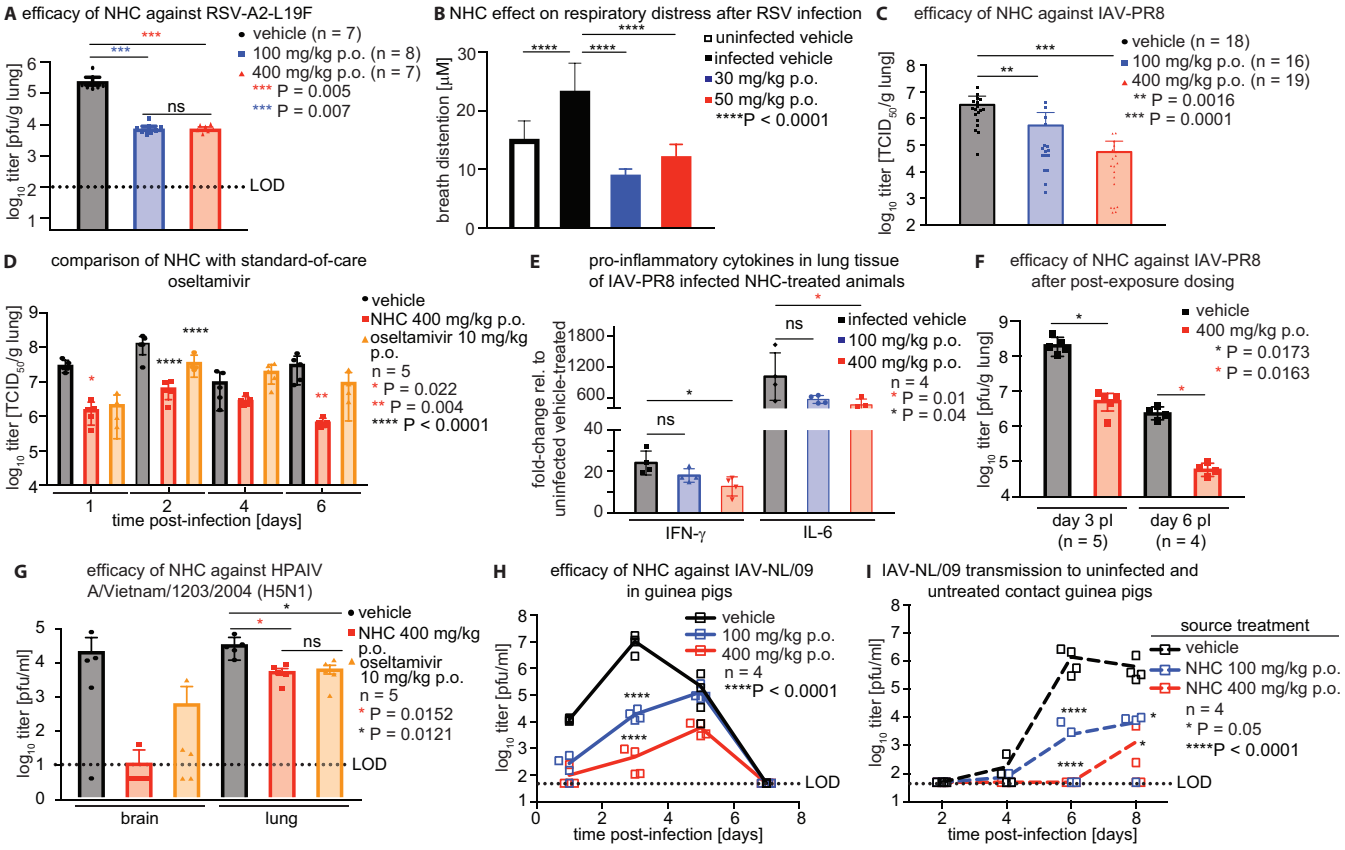

FIG 4 *In vivo* efficacy of NHC. (A to F) BALB/cJ mice were infected i.n. with 1×10^5 PFU of RSV-A2-L19F (A and B) or 1,000 PFU of IAV-PR8 (C to F), and NHC was dosed orally b.i.d. Symbols represent individual biological repeats, and columns show mean values ± SD. LOD, limit of detection. (A) Lung RSV loads were determined at 5 days postinfection through immunoplaque assays. Dosing was initiated prophylactically at 2 h preinfection. Statistical significance was determined by one-way ANOVA with Tukey's *post hoc* test. (B) Breath distension of peripheral arteries was quantified 8 days after infection with RSV through pulse oximetry. Control animals were mock infected and vehicle treated. Statistical significance was determined by one-way ANOVA with Tukey's *post hoc* test. (C) Lung IAV-PR8 loads were determined at 6 days postinfection. Dosing was initiated prophylactically. Statistical significance was determined by one-way ANOVA with Dunnett's *post hoc* test. (D) Comparison of NHC with the SOC oseltamivir. Lung IAV-PR8 loads were determined on the specified days postinfection. Dosing was initiated prophylactically. Statistical significance was determined by two-way ANOVA with Tukey's *post hoc* test. (E) Relative expression levels of the proinflammatory cytokines IFN-γ and IL-6 in lung tissue of IAV-PR8-infected animals were quantified by RT-qPCR at 3 days postinfection and are expressed relative to values for uninfected, vehicle-treated animals. Statistical significance was determined by one-way ANOVA with Dunnett's *post hoc* test. (F) Postexposure dosing of NHC, initiated at 6 h postinfection. Lung IAV-PR8 loads were determined at 3 and 6 days postinfection. Statistical significance was determined by unpaired *t* tests with Welch's correction for each time point. (G) Oral efficacy of NHC against HPAIV. Mice were infected with 6 PFU of A/Vietnam/1203/2004 (H5N1), and brain and lung virus loads were determined at 6 days postinfection. Treatment was initiated prophylactically at 2 h preinfection; statistical significance was determined by one-way ANOVA with Tukey's *post hoc* test. (H and I) Oral NHC efficacy and suppression of virus transmission in guinea pigs. (H) Source animals were infected i.n. with 10^4 PFU of IAV-NL/09, and virus loads in nasal lavage fluids were determined on days 1, 3, 5, and 7 postinfection. Treatment was initiated prophylactically at 2 h preinfection and continued b.i.d. to the end of day 3 postinfection. (I) Untreated and uninfected contact animals were added at 24 h postinfection, and transmitted virus titers in nasal lavage fluids were determined on days 2, 4, 6, and 8. Analysis was done with two-way ANOVA and Dunnett's *post hoc* test.

oseltamivir-treated animals, but NHC more efficiently prevented HPAIV dissemination to the CNS, since three of the five animals in the oseltamivir treatment group presented with detectable virus in brain tissue.

Since influenza virus does not transmit efficiently in mice (47), we employed the well-established guinea pig IAV transmission model (48) to evaluate the effect of NHC on virus spread. Similar to uncomplicated human influenza, virus replication in guinea pigs is limited predominantly to the upper respiratory tract. Source animals were infected i.n. with 10^4 PFU of A/Netherlands/602/2009 pH1N1 (NL/09) virus and co-housed with uninfected contact guinea pigs starting at 24 h postinfection. Treatment of the source group was initiated prophylactically at the 100- and 400-mg/kg dose levels and continued b.i.d. as described above. Source animals showed a significant, dose-dependent reduction in shedding titers determined from nasal lavage specimens that exceeded 2 orders of magnitude (Fig. 4H). Vehicle-treated animals furthermore

efficiently passed the virus to contact guinea pigs. Transmitted virus was first detected at day 4 postinfection, and titers peaked at approximately 10^6 PFU/ml of nasal wash fluid on day 6 after the initiation of the study. In contrast, low-dose NHC treatment of source guinea pigs delayed transmission by approximately 1 day, and titers remained below 10^4 PFU/ml of nasal wash fluid throughout the study (Fig. 4l). We noted an even more pronounced inhibitory effect on virus spread when source animals were treated at the 400-mg/kg dose level. Weak transmission was detected in this group only at day 8 and remained limited to two of the four contacts. The other contact animals remained virus-free for the duration of the study. These studies demonstrate the oral efficacy of NHC against major pathogens associated with influenza-like illnesses in different animal models.

DISCUSSION

Influenza-like illnesses show disproportionally high case fatality rates in older adults (1–3). To effectively address this problem, a next-generation therapeutic must be developed for this patient population frequently suffering from seasonal influenza virus or RSV infection and presenting with influenza-like symptoms. In addition to a reduction in viral loads that is sufficient to prevent disease progression to severe small airway infection and alleviate acute respiratory distress, a drug candidate suitable for this patient group should best be orally available to ensure reasonable patient compliance.

Through a dual-pathogen (31, 32) HTS campaign that affords the simultaneous identification of RSV and IAV inhibitors, we identified NHC, a pyrimidine ribonucleoside analog, as a hit candidate that integrates promising potency with a broadened indication spectrum. NHC was previously associated with antiviral activity against positive-strand RNA viruses (36–39), but PK/PD profiles have not been determined, and *in vivo* efficacy is untested.

The broad overall indication spectrum of NHC is reminiscent of those described for T-705 (favipiravir) and ribavirin, two compounds that act after phosphoribosylation (T-705) and phosphorylation as purine analogs, respectively, and are believed to interfere with RNA virus replication through pairing with either cytidine or uridine (49, 50), resulting in high mutation frequencies and, ultimately, error catastrophe (42). While T-705 is conditionally approved in Japan and considered for licensing in the United States, we found the drug to be compromised by poor antiviral activity in primary human respiratory cells. In contrast, NHC returned a consistent efficacy profile in immortalized cell lines and in disease-relevant primary HBTECs, consistent with efficient conversion to active NHC-TP and the high metabolic stability of the 5′-triphosphate also in primary human airway cells.

Early studies suggested that NHC-TP can substitute for uridine or cytidine in RNA polymerase reactions (51, 52). Three lines of experimental evidence support our hypothesis that the anti-influenza virus and anti-RSV activity of NHC is predominantly the result of viral error catastrophe: (i) an excess of exogenous cytidine or uridine but not purine reverses compound-mediated inhibition, indicating that NHC is recognized as a pyrimidine analog by the influenza virus and RSV RdRp complexes; (ii) NHC-TP can functionally substitute for CTP in a biochemical RSV polymerase assay using purified RdRp complexes; and (iii) growth of IAV-WSN and RSV-A2-L19F in the presence of substerilizing NHC concentrations resulted in an increased frequency of C-to-U, G-to-A, and A-to-G transition mutations.

Data from the cell-based competition assays indicate that substrate recognition of NHC-TP by RSV and IAV polymerases is comparable to that of CTP, since at least equimolar concentrations of exogenous cytidine were required to reverse NHC-mediated inhibition despite the micromolar levels of endogenous ribonucleosides naturally present in the cells (53). Previous mutagenesis studies with both positive- and negative-sense RNA viruses have shown that viral tolerance for an increased mutation frequency is limited (50, 54–56). For instance, an average of three random mutations per viral genome is sufficient for an 80% reduction in poliovirus specific infectivity (42). In our biochemical assays, however, NHC-TP only partially restored RSV polymerase

activity in the absence of CTP. This finding suggests that the incorporation of the compound may also reduce polymerase processivity and/or increase the likelihood of chain termination. Of note, T-705 was also suggested to directly block influenza virus RdRp (57), and a number of alternative antiviral effects were suggested for ribavirin, including decreased cellular GTP levels, immunomodulation, blockage of RNA capping, and direct viral polymerase inhibition (58). Conceivably, the antiviral activity of NHC may arise from a combination of lethal mutagenesis and kinetically impaired or abortive polymerization.

Previous work predicted a mutagenic effect of NHC based on the restored growth of the cytidine auxotroph *Salmonella enterica* serovar Typhimurium JL1045 after exposure to the compound (59). However, this conclusion is flawed, since NHC can be converted directly to cytidine by the mitochondrial amidoxime-reducing component (mARC) (60); thus, the drug itself and not compound-induced reversion mutants serves as the pyrimidine source for JL1045. Consistent with this view, DNA repair mechanisms are not activated by NHC (61). Furthermore, the anticipated treatment time for influenza and RSV disease is short—the recommended course of oseltamivir, for instance, is 5 to 7 days (14)—and prolonged exposure to NHC was well tolerated by both mice and guinea pigs.

Consistent across both positive- and negative-strand viral targets pursued, viral escape from inhibition by NHC remains inefficient, and extended passaging under conditions that we have successfully optimized in previous studies for the induction of resistance to allosteric antivirals (32, 62, 63) failed to yield appreciably higher tolerance to NHC. A recent study aimed at inducing the escape of Venezuelan equine encephalitis virus (VEEV), a *Togaviridae* family member, from NHC inhibition found that a combination of three distinct mutations in VEEV RdRp was required for partial escape (36). However, subsequent viral passaging in the absence of the compound resulted in a rapid loss of resistance. The appearance of preexisting resistance to available antivirals in circulating influenza viruses is a major concern, having compromised the M2 ion channel blocker class (64) and affecting, increasingly, the neuraminidase inhibitors (65–69). Although we have not yet determined *in vivo* resistance profiles of the compound, the available data in aggregate suggest that a fitness penalty may prevent the rapid accumulation of preexisting anti-NHC resistance mutations.

Based on PK profiles in mice indicating sustained high lung tissue concentrations of the antivirally active NHC-TP anabolite, we chose the mouse models of RSV and IAV infection for small-animal efficacy testing. While supporting productive infections, the tissue tropism differs from that of human disease in both models since virus replication occurs predominately in the small airways rather than the upper respiratory tract (70–73). In the case of the IAV model, mice furthermore develop hypothermia rather than fever (74) and do not cough or sneeze (47). In keeping with our overall therapeutic premise that reducing the progeny viral load will be paramount in preventing viral spread to the small airways and severe lower respiratory tract infection in humans, we consider the lung viral burden to represent the most relevant readout to assess treatment efficacy in these models, although additional disease biomarkers were monitored in parallel. The observed significant lung virus load reductions were consistent with efficient NHC uptake and anabolism in primary cells, the antiviral activity of the compound in native cell cultures and *in ovo*, and the sustained lung tissue concentrations of NHC-TP in mice. Virus titer reductions were equivalent to, or exceeded, those reported previously for the SOCs ribavirin (75) and oseltamivir (45) in the mouse model.

Clinical studies and animal models have implicated a number of proinflammatory mediators in playing a significant role in coordinating the innate immune response to influenza virus infection (76–78). IL-6 in particular was identified as a promising biomarker for disease severity in the PR8 BALB/cJ model based on the correlation of IL-6 levels with viral titers (45, 79). Consistent with viral load reductions in NHC-treated animals, we found that relative IL-6 expression levels were significantly reduced in the

high-dose NHC treatment group, underscoring the therapeutic benefit of the compound against influenza.

No robust small-animal RSV transmission model is available, but guinea pigs support efficient IAV transmission. Although lacking overt signs of disease, guinea pigs are highly susceptible to infection by human influenza viruses. Virus replication to high titers in the guinea pig upper respiratory tract, resembling a hallmark of uncomplicated influenza in humans, furthermore generates a basis for efficient direct and aerosol transmission (48). In addition to substantially lower viral loads in treated source animals that corroborated the results of the mouse efficacy studies, the reduced IAV transmission success under NHC treatment generates high promise that human therapy with NHC may accelerate the silencing of virus outbreaks in addition to improving the management of influenza-like disease.

NHC emerges from this first *in vivo* efficacy assessment study as an orally active ribonucleoside analog with potent activity against influenza viruses and RSV. The compound was highly bioavailable, efficiently converted to the active NHC-TP form in disease-relevant respiratory tissues, and well tolerated and did not induce rapid viral escape from inhibition. NHC was effective against seasonal and highly pathogenic avian IAV strains, IBV strains, and RSV isolates in cell culture. Treatment alleviated clinical markers of RSV and influenza virus disease in the mouse model and effectively reduced influenza virus host-to-host spread in a guinea pig transmission model. We consider NHC or a prodrug analog thereof to be worthwhile for further consideration as a promising candidate for the treatment of influenza-like diseases.

MATERIALS AND METHODS

Cell lines and transfections. Human embryonic kidney cells (293T; ATCC CRL-3216), Madin-Darby canine kidney (MDCK) cells (ATCC CCL-34), HEp-2 cells (ATCC CCL-23), and baby hamster kidney cells (BHK-21; ATCC CCL-10) stably expressing T7 polymerase (BSR-T7/5) were maintained at 37°C and 5% CO_2 in Dulbecco's modified Eagle's medium (DMEM) supplemented with 7.5% fetal bovine serum (FBS). HEp-2 cells are listed in the ICLAC database, version 8.0, of commonly misidentified cell lines, but their use is justified, as these cells are accepted and widely used for studies involving respiratory syncytial virus (RSV). GeneJuice transfection reagent (Invitrogen) was used for all transfection reactions. Normal primary human bronchial tracheal epithelial cells (HBTECs) (purchased from LifeLine Cell Technology [catalog no. LM-0050], passages 1 to 3) were grown in BronchiaLife cell culture medium (LifeLine Cell Technology). Immortalized cell lines used in this study are routinely checked for microbial contamination (in approximately 6-month intervals). HBTECs were tested for microbial contamination on 25 July 2017 by LifeLine Cell Technology. HBTEC passage numbers 2 and 3 were used for this study.

Viruses. Influenza viruses A/WSN/33 (WSN) (H1N1), WSN-nanoLuc, A/California/7/2009 (H1N1), A/Georgia/M5081/2012 (H1N1), A/Netherlands/602/2009 (H1N1), A/Panama/2007/99 (H3N2), A/Wisconsin/67/2005 (H3N2), A/Aichi/2/68 (H3N2), A/swine/Ohio/sw10-132/2010 (H3N2), B/Yamagata/16/88, and B/Brisbane/60/08 were propagated in MDCK cells for 2 days at 37°C. Influenza viruses A/duck/Alberta/35/76 (H1N1), A/swine/Spain/53207/2004, and A/chicken/Potsdam/178-4/83 (H2N2) were propagated in 10-day-old embryonated chicken eggs for 2 days at 37°C. Influenza viruses A/Vietnam/1203/2004 (H5N1) and A/Anhui/1/2013 (H7N9) were propagated in 9-day-old embryonated chicken eggs at 37°C for 24 h. All experiments using live, highly pathogenic H7N9 avian influenza viruses were reviewed and approved by the institutional biosafety program at the University of Georgia, were conducted in biosafety level 3 enhanced containment and followed guidelines for the use of select agents approved by the CDC. Viruses were titrated by standard plaque assays, hemagglutination assays (80), 50% tissue culture infective dose ($TCID_{50}$) assays, or $TCID_{50}$-hemagglutination ($TCID_{50}$-HA) assays in MDCK cells. For $TCID_{50}$-HA assays, 10-fold serial dilutions of virus samples in eight replicates each were propagated for 48 h on MDCK cells in a 96-well plate format, followed by the transfer of culture supernatants to suspensions of chicken red blood cells and scoring of individual wells based on hemagglutination activity. Clinical RSV isolates were collected from patient nasal wash specimens in 2010, cultured on primary rhesus monkey kidney (RhMK) cells, and amplified once on HEp-2 cells prior to use in this study. Recombinant RSV and RSV isolates were grown in HEp-2 cells and titrated by a plaque or immunoplaque assay in HEp-2 cells.

Purification of recombinant reporter virus stocks. Progeny virions were collected from cell culture supernatants (IAV) or released from infected cells through one freeze-thaw cycle (RSV) and subjected to a clearance centrifugation (4,000 rpm for 20 min at 4°C). Virions were diluted in DMEM, purified through a 20% to 60% one-step sucrose gradient in TNE buffer (1 mM Tris [pH 7.2], 100 mM NaCl, 10 mM EDTA) (30,000 rpm for 120 min at 4°C), and harvested from the gradient intersection. Purified virus stocks were stored in aliquots at −80°C.

Automated drug screening. MDCK cells were injected into barcoded white-walled/clear-bottomed 384-well plates by using a MultiFlo automated dispenser (BioTek) equipped with dual 10-μl peristaltic pump manifolds and incubated for 5 h at 37°C and 5% CO_2. Compounds were added to a final

concentration of 5 μM (20 nl/well) by using a high-density pin tool (V&P Scientific), followed by coinfection with recRSV-A2-L19F-fireSMASh (multiplicity of infection [MOI] = 0.1) and recIAV-nanoLuc (MOI = 0.02) at 10 μl/well by use of a MultiFlo dispenser unit and incubation for 48 h at 37°C and 5% CO_2. The final vehicle (dimethyl sulfoxide [DMSO]) concentration was 0.05%. The reporter gene activity was recorded at 48 h postinfection with an H1 synergy multimode plate reader (BioTek), and compounds showing ≥80% inhibition of both RSV and IAV were pursued as hit candidates. The MScreen software package was used for library management and campaign analysis.

Dose-response antiviral activity and cytotoxicity testing in cultured cells. For automated dose-response testing, 3-fold serial dilutions were prepared in 96-well plates in three replicates each by using a Nimbus liquid handler (Hamilton). Target cells, as specified, were seeded into white-wall clear-bottom 96-well plates (8×10^3 cells/well), and the serial dilutions were transferred by using the liquid handler, followed by infection with IAV-WSN-nanoLuc (MOI = 0.02) or RSV-A2-L19F-fireSMASh (MOI = 0.1). Reporter signals were recorded with the H1 synergy plate reader as described above. To determine cell viability, the PrestoBlue substrate (5 μl/well; Life Technologies) was added after 48 h of incubation of compound-exposed uninfected cells at 37°C, and top-read fluorescence (excitation at 560 nm, emission at 590 nm, and instrument gain of 85) was recorded after incubation for 45 min at 37°C by using the H1 synergy plate reader. Raw data for all automated dose-response assays were analyzed according to the formula % inhibition = $(X_{Sample} - X_{Min})/(X_{Max} - X_{Min}) \times 100$, with X_{Min} representing the average of data from four positive-control (1 mg/ml cycloheximide) wells and X_{Max} representing the average of data from four negative-control (DMSO) wells included on each plate. Four-parameter variable-slope regression modeling was applied to determine 50% active (EC_{50}) and toxic (CC_{50}) concentrations, using the nonlinear regression function in the Prism software package (GraphPad). For manual dose testing of nonreporter viruses, target cells were seeded into 12-well plates (1.5×10^5 cells/well) and, at approximately 90% confluence, infected with the test virus in the presence of serial compound dilutions. Progeny virus titers were determined at 36 to 48 h postinfection, depending on the virus strain analyzed, and viral titers were determined as described above.

Human DNA polymerase inhibition assay. Inhibition of human DNA polymerase α was assayed in a 96-well format in wells containing reaction buffer [50 mM Tris-HCl (pH 8.7), 10 mM $MgCl_2$, 0.4 mg/ml bovine serum albumin (BSA), 1 mM dithiothreitol (DTT), 15% glycerol, 0.05 mM dCTP, 0.05 mM dTTP, 0.05 mM dATP, 10 μCi [α-^{32}P]dGTP (800 Ci/mmol)], 20 μg activated calf thymus DNA, and NHC-TP in a range of different concentrations. Aphidicolin served as a polymerase inhibitor reference. Reactions were carried out for 30 min at 37°C, followed by transfer to filter plates, precipitation with 10% trichloroacetic acid, and repeated washing with 5% trichloroacetic acid and 95% ethanol. The incorporation of [α-^{32}P]GTP was measured after filter drying using a Microbeta scintillation counter.

Efficacy against IAV *in ovo*. Serum-pathogen-free (SPF) freshly fertilized chicken eggs were purchased from Hy-Line and incubated at 37°C with 55 to 60% humidity for 10 to 11 days. Eggs were candled and disinfected with 70% ethanol, and NHC in sterile phosphate-buffered saline (PBS) was administered to a final concentration of approximately 10 μM directly into the allantoic fluid 2 h prior to infection by using a 22-gauge needle. The average volume of the allantoic fluid was considered to be 50 ml. Eggs were sealed and incubated for 2 h, followed by infection with 10 HA units of A/Swine/Spain/53207/2004 (H1N1). After a 48-h incubation, eggs were cooled to 4°C, and virus was harvested from the allantoic fluid and titrated by using standard HA assays and turkey red blood cells.

Replicon reporter assays. Reporter activities were determined in the presence of 3-fold serial dilutions of NHC starting from 20 μM for RSV and 100 μM for IAV; treatment was initiated immediately after transfection. Luciferase activities in cell lysates were measured with a Synergy H1 microplate reader (BioTek) in the top-count mode using a Dual-Glo luciferase assay system (Promega). Inhibitory concentrations were calculated through four-parameter variable-slope regression modeling.

Time-of-addition variation studies. HEp-2 cells were infected with RSV-A2-fireSMASh at an MOI of 0.1, and MDCK cells were infected with IAV WSN-nanoLuc at an MOI of 0.05. At the specified time points relative to infection, NHC, GRP-71271, AL-8176, or CL-309623 was added to the culture media to a final concentration of 10 μM. T-705 was added to a final concentration of 50 μM, and equivalent volumes of DMSO served as vehicle controls. Reporter gene expression was measured at 24 h (IAV-WSN-nanoLuc) or 48 h (RSV-A2-fireSMASh) postinfection, and the obtained values were expressed relative to the values for the vehicle-treated samples.

Nucleotide competition experiments. HEp-2 cells were infected with RSV-A2-fireSMASh at an MOI of 0.1, and MDCK cells were infected with IAV-WSN-nanoLuc at an MOI of 0.05. At the time of infection, NHC was added to a final concentration of 10 μM NHC alone or in combination with 0.1 to 300 μM exogenous nucleosides (Sigma-Aldrich). Volume equivalents of DMSO served as vehicle controls. Reporter gene expression was quantified at 24 h (IAV-WSN-nanoLuc) or 48 h (RSV-A2-fireSMASh) postinfection. Values are expressed relative to the values for the vehicle-treated samples.

***In vitro* RSV polymerase assay.** RSV large polymerase subunit (L) and phosphoprotein (P) complexes were expressed from a baculovirus vector and purified by affinity chromatography: L-P complexes were eluted from a Ni-nitrilotriacetic acid (NTA) column with 250 mM imidazole in a solution containing 50 mM NaH_2PO_4 (pH 7.5), 150 mM NaCl, and 0.5% NP-40, followed by dialysis against a solution containing 150 mM NaCl, 20 mM Tris-HCl (pH 7.4), 1 mM DTT, and 10% glycerol. L-P hetero-oligomers were mixed in Mg^{2+} buffer with a 25-mer RNA oligonucleotide template containing essential RSV promoter sequences and rNTPs (ribonucleotide triphosphate), including 0.07 μM [α-^{32}P]UTP tracer but lacking CTP. NHC, NHC-TP, or CTP was added as specified. Predominant initiation at the +3 position results in up to 23-mer

radiolabeled amplicons, which were subjected to denaturing gel electrophoresis, followed by autoradiography.

Assessment of mutation frequencies in viral RNA. HEp-2 cells were infected with RSV-A2-mKate at an MOI of 0.1, and MDCK cells were infected with IAV-WSN at an MOI of 0.05, followed by growth in the presence of 10 μM NHC for 24 h; equivalent volumes of DMSO were used as vehicle controls. Total RNA was extracted by using the ZR viral RNA kit (Zymo Research), and cDNA of the viral message was synthesized with SuperScript III reverse transcriptase (Thermo Scientific) and oligo(dT) primers. The PB1 segment of IAV-WSN or an ~1,500-nucleotide fragment of the RSV-A2-mKate L open reading frame (ORF) was amplified by PCR and subcloned into the pUC19 vector. For each virus and treatment condition, at least 10 distinct subclones (equaling in aggregate at least approximately 7,500 nucleotides each) were Sanger sequenced by using universal M13 primers. Data were analyzed with the Sequencer package, and mutation frequencies were expressed per 5,000 nucleotides for IAV-WSN and per 10,000 nucleotides for RSV-A2. Fisher's exact test was used for statistical analyses.

Virus adaptation in cell culture. Both dose escalation and fixed-dose adaptation strategies were applied. For dose escalation, MDCK cells were infected with IAV-WSN at an MOI of 0.01, and HEp-2 cells were infected with RSV-A2-mKate at an MOI of 0.1. The viruses were passaged in the presence of increasing concentrations of NHC, starting at 250 nM. Dose concentrations were doubled at virus passage up to a final concentration of 10 μM. Six independent passage lines each per target virus were advanced simultaneously for a total of 10 passages, each entailing virus harvest from infected cells, dilution, and reinfection of fresh cell populations in the presence of the compound or vehicle. Virus titers declined significantly toward the end of the series, and no resistant variants emerged. For fixed-dose adaptation, MDCK cells were infected with IAV-WSN or B/Brisbane/60/08 at an MOI of 0.01, and HEp-2 cells were infected with RSV-A2-mKate at an MOI of 0.1. The viruses were passaged in the presence of EC_{99} equivalents of NHC for the respective target viruses, as described above, for a total of 10 passages. Progeny virus titers again declined toward the end of the cycle, and no drug-resistant virus population could be cultivated.

Anabolism and turnover in cultured cells. To screen for cellular uptake and anabolism of NHC to NHC-TP, HBTECs were grown in the presence of 20 μM NHC for 0, 1, 2, 3, 4, 6, 16, and 24 h. Cells were washed with PBS and lysed with 70% methanol, and clarified samples were stored at −20°C until analysis. To determine the stability of NHC-TP and other anabolites, HBTECs were grown in the presence of 20 μM NHC for 24 h, medium was changed to drug-free BronchiaLife cell culture medium, and cells were incubated for an additional 0, 0.5, 1, 2, 3, and 6 h. Metabolites were extracted with 70% methanol as described above, and samples were kept at −20°C until analysis. NHC anabolites were quantitated by using internal standard-based LC-MS/MS on an Agilent 1200 system (Agilent Technologies) equipped with a SeQuant ZIC-pHILIC column (The Nest Group). Mass spectrometry analysis was performed on a QTrap 5500 mass spectrometer (AB Sciex) using negative-mode electrospray ionization (ESI) in the multiple-reaction-monitoring (MRM) mode. Data analysis was performed by using Analyst software (AB Sciex).

PK and PD studies in mice. Female CD-1 mice (6 to 8 weeks of age) distributed randomly into groups were dosed p.o. with NHC in 240 mM citrate buffer, followed by blood and lung tissue sampling. Plasma was purified from heparinized blood, and tissue samples were snap-frozen prior to 70% acetonitrile extraction. Drug concentrations were determined by using $^{13}C_5$-labeled internal standards for NHC and NHC-TP. Mass spectrometry was performed as detailed above. For calibration, standard curves were prepared in blank plasma (concentration range, 25 to 30,000 ng/ml) and blank tissue lysate (concentration range, 1.49 to 1,490 ng/ml). Quality control samples of 30, 500, and 900 ng/ml in blank plasma were analyzed at the beginning of the analysis of each sample set. Calibration in each matrix showed linearity with R^2 values of >0.99.

Mouse model for RSV infection. Female BALB/cJ mice (5 to 6 weeks of age) were obtained from the Jackson Laboratory or Envigo, rested for 1 week, assigned to groups randomly, anesthetized by intraperitoneal injection of a ketamine-xylazine solution, and infected i.n. with 1×10^5 PFU of recRSV-A2-L19F. NHC was administered orally in 240 mM citrate buffer or an equivalent volume of the vehicle at 2 h preinfection, and dosing continued b.i.d. for up to 8 days. For virus load titration, lungs were extracted and homogenized, homogenates were serially diluted and transferred to HEp-2 cells, and cells were overlaid at 1 h postinfection with minimum essential medium (MEM) containing 10% FBS, penicillin G, streptomycin sulfate, an amphotericin B solution, and 0.75% methylcellulose. At 6 days postinfection, cells were fixed with methanol, and plaques were visualized by immunodetection. To quantify mucin expression, mice were euthanized at 8 days postinfection, and heart-lung tissue was harvested and fixed in 10% formalin. Lung tissue sections embedded in paraffin blocks were stained with periodic acid-Schiff (PAS) stain, and slides were digitally scanned by using a Zeiss Mirax Midi microscope (Carl Zeiss Microimaging). To determine respiratory distress noninvasively, a rodent pulse oximeter (MouseOx; Starr Life Sciences Corp., Oakmont, PA) was applied to the mouse's thigh, and arterial O_2 saturation, heart rate, pulse rate, pulse distension, and breath distension were measured every 0.1 s for a 1- to 5-min overall period. The mean breath distension for each treatment group was calculated based on mean values of all measurements for each animal in which all target parameters were present.

Mouse model for IAV infection. Female BALB/cJ mice (6 to 8 weeks of age) were received from Envigo and housed in ABSL-2 (animal biosafety level; for infection with IAV-PR8) or ABSL-3 (for infection with HPAIV) facilities in HEPA-filtered microisolator caging. Mice were rested for 1 week, weighed, assigned to groups randomly, and infected with 10^3 PFU of IAV-PR8 or 6 PFU of A/Vietnam/1203/04 (H5N1), as specified, in PBS. Treatment was initiated at 2 h preinfection (prophylactic dosing) or 6 h postinfection (therapeutic dosing) and continued for up to 6 days b.i.d. Compounds or equivalent volumes of the vehicle were administered orally in a 240 mM citrate buffer formulation. Animal clinical signs were

tracked daily, and animals were euthanized at the indicated time points or when humane endpoints were reached. Lung and, where indicated, brain tissue were removed, homogenized, and clarified by centrifugation, and aliquots were frozen at −80°C, as outlined above, until virus titration was performed.

Induction of select cytokine mRNAs in mouse lung tissue. Relative IFN-γ and IL-6 induction levels present in mouse lung tissue were determined by semiquantitative real-time PCR analysis. Total RNA was extracted from lung tissue 3 days after infection of animals with IAV-PR8 or mock infection (representing day 0). Infected animals were treated orally with NHC or equivalent volumes of the vehicle (citrate buffer). RNA was reverse transcribed with SuperScript III reverse transcriptase, and the resulting cDNAs were subjected to real-time PCR using Fast SYBR green master mix (Applied Biosystems). Glyceraldehyde-3-phosphate dehydrogenase (GAPDH) mRNA served as an internal control, and mRNA induction levels were normalized to the average of the values obtained for mock-infected animals. Each biological repeat was determined in duplicate, and relative changes in transcription levels were calculated according to fold changes determined by the $2^{-\Delta\Delta C_T}$ method.

Guinea pig IAV infection-and-transmission model. Female Hartley strain guinea pigs weighing 250 to 300 g were obtained from Charles River Laboratories. The animals were assigned to groups randomly, and prior to intranasal inoculation, nasal lavage, or CO_2 euthanasia, the guinea pigs were sedated with a mixture of ketamine and xylazine (30 mg/kg of body weight and 4 mg/kg, respectively). Inoculation and nasal lavage were performed with PBS as the diluent/collection fluid in each case. Oral treatment of infected donor animals with NHC or the vehicle (240 mM citrate buffer with Ora-Sweet [Paddock Laboratories]) was initiated at 2 h preinfection and continued b.i.d. until the end of day 3 postinfection. Following inoculation and recovery from sedation, donor guinea pigs were housed in Caron 6040 environmental chambers (fitted with the optional dryer package) set to 10°C and 20% relative humidity. Twenty-four hours after inoculation of the donor animals, exposed guinea pigs were introduced into the donor animal cages. Conditions of 10°C and 20% relative humidity were maintained throughout the exposure period, which ended on day 8 postinoculation. Titers of virus shedding in nasal lavage fluids of source and contact animals were determined through plaque assays.

Statistical analysis. To assess experimental variation and the statistical significance of differences between sample means, one-way or two-way analysis of variance (ANOVA) was carried out in combination with Tukey's, Dunnett's, or Sidak's *post hoc* test, as specified in the figure legends, using the Prism software package (GraphPad). Fisher's exact test was used for statistical analyses of mutation frequencies. Results for individual biological replicates are shown for all *in vivo* efficacy experiments. When appropriate, experimental uncertainties are identified by error bars, representing standard deviations (SD).

IACUC approval statement. All animal work was performed in compliance with the *Guide for the Care and Use of Laboratory Animals* of the National Institutes of Health (81). Mouse work at Georgia State University was approved by the GSU Institutional Animal Use and Care Committee (IACUC) under protocol A17019; mouse and guinea pig work at Emory University was approved by the Emory IACUC under protocol no. DAR-2003089-ENTRPR-N and DAR-2002738-ELMNTS-A, respectively; and mouse studies with HPAIV at the University of Georgia were approved by the UGA IACUC under protocol no. A2017 05-009.

SUPPLEMENTAL MATERIAL

Supplemental material for this article may be found at https://doi.org/10.1128/AAC.00766-18.

SUPPLEMENTAL FILE 1, PDF file, 2.3 MB.

ACKNOWLEDGMENTS

We thank A. Mehle and S. Schultz-Cherry for IAV H5N1 and H7N9 minigenome reporter systems, K. K. Conzelmann for the BSR-T7/5 cell line, C. Jones, S. Johnson, and C. Kyriakis for assistance with the murine HPAIV studies, G. P. Reddy, J. Marlow, and J. DeBergh for assistance with bioanalytical analysis, ImQuest BioSciences for assistance with the human DNA polymerase assay, L. Martinez-Sobrido for IBV isolates, R. T. Jacob for IT support, and A. L. Hammond for critical reading of the manuscript. The MScreen software package was kindly provided by the Center for Chemical Genomics of the University of Michigan under a license agreement by the University of Michigan Office of Technology Transfer; JChem was used for structure database management, search, and prediction (JChem 6.2, 2014; ChemAxon); and Marvin was employed for drawing, displaying, and characterizing chemical structures, substructures, and reactions (Marvin 14.9.22.0, 2014; ChemAxon).

This work was supported, in part, by contracts HDTRA1-15-C-0075 and HHSN272201500008C from the DTRA and the NIH/NIAID, respectively (to G.R.P.), and by Public Health Service grants AI119196, AI071002, and HD079327 from the NIH/NIAID and NIH/NICHD, respectively (to R.K.P.). The funders had no role in study design, data collection and interpretation, or the decision to submit the work for publication.

We declare no competing interests.

REFERENCES

1. Zhou H, Thompson WW, Viboud CG, Ringholz CM, Cheng PY, Steiner C, Abedi GR, Anderson LJ, Brammer L, Shay DK. 2012. Hospitalizations associated with influenza and respiratory syncytial virus in the United States, 1993-2008. Clin Infect Dis 54:1427–1436. https://doi.org/10.1093/cid/cis211.
2. Falsey AR, Hennessey PA, Formica MA, Cox C, Walsh EE. 2005. Respiratory syncytial virus infection in elderly and high-risk adults. N Engl J Med 352:1749–1759. https://doi.org/10.1056/NEJMoa043951.
3. Thompson WW, Shay DK, Weintraub E, Brammer L, Cox N, Anderson LJ, Fukuda K. 2003. Mortality associated with influenza and respiratory syncytial virus in the United States. JAMA 289:179–186. https://doi.org/10.1001/jama.289.2.179.
4. Stiver G. 2003. The treatment of influenza with antiviral drugs. CMAJ 168:49–56.
5. Skowronski DM, Chambers C, De Serres G, Dickinson JA, Winter A-L, Hickman R, Chan T, Jassem AN, Drews SJ, Charest H, Gubbay JB, Bastien N, Li Y, Krajden M. 2018. Early season co-circulation of influenza A(H3N2) and B(Yamagata): interim estimates of 2017/18 vaccine effectiveness, Canada, January 2018. Euro Surveill 23:pii=18-00035. https://doi.org/10.2807/1560-7917.ES.2018.23.5.18-00035.
6. Broor S, Parveen S, Bharaj P, Prasad VS, Srinivasulu KN, Sumanth KM, Kapoor SK, Fowler K, Sullender WM. 2007. A prospective three-year cohort study of the epidemiology and virology of acute respiratory infections of children in rural India. PLoS One 2:e491. https://doi.org/10.1371/journal.pone.0000491.
7. Mahadevia PJ, Makari D, Masaquel A. 2012. Methodological concerns regarding cost-effectiveness analysis of palivizumab in Florida Medicaid. Arch Pediatr Adolesc Med 166:968–970. https://doi.org/10.1001/archpediatrics.2012.1591.
8. Mahadevia PJ, Masaquel AS, Polak MJ, Weiner LB. 2012. Cost utility of palivizumab prophylaxis among pre-term infants in the United States: a national policy perspective. J Med Econ 15:987–996. https://doi.org/10.3111/13696998.2012.690013.
9. Weiner LB, Masaquel AS, Polak MJ, Mahadevia PJ. 2012. Cost-effectiveness analysis of palivizumab among pre-term infant populations covered by Medicaid in the United States. J Med Econ 15:997–1018. https://doi.org/10.3111/13696998.2012.672942.
10. Kamal-Bahl S, Doshi J, Campbell J. 2002. Economic analyses of respiratory syncytial virus immunoprophylaxis in high-risk infants: a systematic review. Arch Pediatr Adolesc Med 156:1034–1041. https://doi.org/10.1001/archpedi.156.10.1034.
11. Hampp C, Kauf TL, Saidi AS, Winterstein AG. 2011. Cost-effectiveness of respiratory syncytial virus prophylaxis in various indications. Arch Pediatr Adolesc Med 165:498–505. https://doi.org/10.1001/archpediatrics.2010.298.
12. DeVincenzo JP, El Saleeby CM, Bush AJ. 2005. Respiratory syncytial virus load predicts disease severity in previously healthy infants. J Infect Dis 191:1861–1868. https://doi.org/10.1086/430008.
13. El Saleeby CM, Bush AJ, Harrison LM, Aitken JA, Devincenzo JP. 2011. Respiratory syncytial virus load, viral dynamics, and disease severity in previously healthy naturally infected children. J Infect Dis 204:996–1002. https://doi.org/10.1093/infdis/jir494.
14. Fiore AE, Fry A, Shay D, Gubareva L, Bresee JS, Uyeki TM, Centers for Disease Control and Prevention. 2011. Antiviral agents for the treatment and chemoprophylaxis of influenza—recommendations of the Advisory Committee on Immunization Practices (ACIP). MMWR Recommend Rep 60:1–24.
15. Salerno D, Hasham MG, Marshall R, Garriga J, Tsygankov AY, Grana X. 2007. Direct inhibition of CDK9 blocks HIV-1 replication without preventing T-cell activation in primary human peripheral blood lymphocytes. Gene 405:65–78. https://doi.org/10.1016/j.gene.2007.09.010.
16. Schang LM. 2006. First demonstration of the effectiveness of inhibitors of cellular protein kinases in antiviral therapy. Expert Rev Anti Infect Ther 4:953–956. https://doi.org/10.1586/14787210.4.6.953.
17. Prussia A, Thepchatri P, Snyder JP, Plemper RK. 2011. Systematic approaches towards the development of host-directed antiviral therapeutics. Int J Mol Sci 12:4027–4052. https://doi.org/10.3390/ijms12064027.
18. Kaufmann SHE, Dorhoi A, Hotchkiss RS, Bartenschlager R. 22 September 2017. Host-directed therapies for bacterial and viral infections. Nat Rev Drug Discov https://doi.org/10.1038/nrd.2017.162.
19. Shaw ML. 2017. The next wave of influenza drugs. ACS Infect Dis 3:691–694. https://doi.org/10.1021/acsinfecdis.7b00142.
20. Dahlin JL, Walters MA. 2014. The essential roles of chemistry in high-throughput screening triage. Future Med Chem 6:1265–1290. https://doi.org/10.4155/fmc.14.60.
21. Baell J, Walters MA. 2014. Chemistry: chemical con artists foil drug discovery. Nature 513:481–483. https://doi.org/10.1038/513481a.
22. Baell JB, Holloway GA. 2010. New substructure filters for removal of pan assay interference compounds (PAINS) from screening libraries and for their exclusion in bioassays. J Med Chem 53:2719–2740. https://doi.org/10.1021/jm901137j.
23. Webster RG, Govorkova EA. 2014. Continuing challenges in influenza. Ann N Y Acad Sci 1323:115–139. https://doi.org/10.1111/nyas.12462.
24. Voss ME, Carter PH, Tebben AJ, Scherle PA, Brown GD, Thompson LA, Xu M, Lo YC, Yang G, Liu RQ, Strzemienski P, Everlof JG, Trzaskos JM, Decicco CP. 2003. Both 5-arylidene-2-thioxodihydropyrimidine-4,6(1H,5H)-diones and 3-thioxo-2,3-dihydro-1H-imidazo[1,5-a]indol-1-ones are light-dependent tumor necrosis factor-alpha antagonists. Bioorg Med Chem Lett 13:533–538. https://doi.org/10.1016/S0960-894X(02)00941-1.
25. Anderson LJ, Parker RA, Strikas RL. 1990. Association between respiratory syncytial virus outbreaks and lower respiratory tract deaths of infants and young children. J Infect Dis 161:640–646. https://doi.org/10.1093/infdis/161.4.640.
26. Groothuis JR, Woodin KA, Katz R, Robertson AD, McBride JT, Hall CB, McWilliams BC, Lauer BA. 1990. Early ribavirin treatment of respiratory syncytial viral infection in high-risk children. J Pediatr 117:792–798. https://doi.org/10.1016/S0022-3476(05)83347-5.
27. Anonymous. 2014. Summary of media conference by Tamura Ministry of Health, Welfare and Labor, on August 15, 2014. Ministry of Health, Welfare and Labor, Tokyo, Japan. (In Japanese.) http://www.mhlw.go.jp/stf/kaiken/daijin/0000054819.html.
28. DeVincenzo J, Fathi H, McClure M, Westland C, Chanda S, Lambkin-Williams R, Smith P, Harrison L, Symons J, Scaglioni-Weinlich C, Zhang Q, Nieforth K, Beigelman L, Blatt L, Fry J. 2014. Treatment with oral ALS-008176, a nucleoside analog, rapidly reduces RSV viral load and clinical disease severity in a healthy volunteer challenge study. Open Forum Infect Dis 1:S66. https://doi.org/10.1093/ofid/ofu083.01.
29. Deval J, Hong J, Wang G, Taylor J, Smith LK, Fung A, Stevens SK, Liu H, Jin Z, Dyatkina N, Prhavc M, Stoycheva AD, Serebryany V, Liu J, Smith DB, Tam Y, Zhang Q, Moore ML, Fearns R, Chanda SM, Blatt LM, Symons JA, Beigelman L. 2015. Molecular basis for the selective inhibition of respiratory syncytial virus RNA polymerase by 2′-fluoro-4′-chloromethylcytidine triphosphate. PLoS Pathog 11:e1004995. https://doi.org/10.1371/journal.ppat.1004995.
30. Yan D, Weisshaar M, Lamb K, Chung HK, Lin MZ, Plemper RK. 2015. Replication-competent influenza virus and respiratory syncytial virus luciferase reporter strains engineered for co-infections identify antiviral compounds in combination screens. Biochemistry 54:5589–5604. https://doi.org/10.1021/acs.biochem.5b00623.
31. Jimenez-Somarribas A, Mao S, Yoon JJ, Weisshaar M, Cox RM, Marengo JR, Mitchell DG, Morehouse ZP, Yan D, Solis I, Liotta DC, Natchus MG, Plemper RK. 2017. Identification of non-nucleoside inhibitors of the respiratory syncytial virus polymerase complex. J Med Chem 60:2305–2325. https://doi.org/10.1021/acs.jmedchem.6b01568.
32. Weisshaar M, Cox R, Morehouse Z, Kumar Kyasa S, Yan D, Oberacker P, Mao S, Golden JE, Lowen AC, Natchus MG, Plemper RK. 2016. Identification and characterization of influenza virus entry inhibitors through dual myxovirus high-throughput screening. J Virol 90:7368–7387. https://doi.org/10.1128/JVI.00898-16.
33. Hoffmann HH, Kunz A, Simon VA, Palese P, Shaw ML. 2011. Broad-spectrum antiviral that interferes with de novo pyrimidine biosynthesis. Proc Natl Acad Sci U S A 108:5777–5782. https://doi.org/10.1073/pnas.1101143108.
34. Krumm SA, Ndungu JM, Yoon JJ, Dochow M, Sun A, Natchus M, Snyder JP, Plemper RK. 2011. Potent host-directed small-molecule inhibitors of myxovirus RNA-dependent RNA-polymerases. PLoS One 6:e20069. https://doi.org/10.1371/journal.pone.0020069.
35. Glezen WP, Schmier JK, Kuehn CM, Ryan KJ, Oxford J. 2013. The burden of influenza B: a structured literature review. Am J Public Health 103:e43–e51. https://doi.org/10.2105/AJPH.2012.301137.
36. Urakova N, Kuznetsova V, Crossman DK, Sokratian A, Guthrie DB,

Kolykhalov AA, Lockwood MA, Natchus MG, Crowley MR, Painter GR, Frolova EI, Frolov I. 22 November 2017. β-D-N^4-Hydroxycytidine is a potent anti-alphavirus compound that induces high level of mutations in viral genome. J Virol https://doi.org/10.1128/JVI.01965-17.
37. Ehteshami M, Tao S, Zandi K, Hsiao HM, Jiang Y, Hammond E, Amblard F, Russell OO, Merits A, Schinazi RF. 2017. Characterization of β-D-N^4-hydroxycytidine as a novel inhibitor of chikungunya virus. Antimicrob Agents Chemother 61:e02395-16. https://doi.org/10.1128/AAC.02395-16.
38. Hollecker L, Choo H, Chong Y, Chu CK, Lostia S, McBrayer TR, Stuyver LJ, Mason JC, Du J, Rachakonda S, Shi J, Schinazi RF, Watanabe KA. 2004. Synthesis of beta-enantiomers of N4-hydroxy-3′-deoxypyrimidine nucleosides and their evaluation against bovine viral diarrhoea virus and hepatitis C virus in cell culture. Antivir Chem Chemother 15:43–55. https://doi.org/10.1177/095632020401500105.
39. Barnard DL, Hubbard VD, Burton J, Smee DF, Morrey JD, Otto MJ, Sidwell RW. 2004. Inhibition of severe acute respiratory syndrome-associated coronavirus (SARSCoV) by calpain inhibitors and beta-D-N4-hydroxycytidine. Antivir Chem Chemother 15:15–22. https://doi.org/10.1177/095632020401500102.
40. Noton SL, Deflube LR, Tremaglio CZ, Fearns R. 2012. The respiratory syncytial virus polymerase has multiple RNA synthesis activities at the promoter. PLoS Pathog 8:e1002980. https://doi.org/10.1371/journal.ppat.1002980.
41. Les A, Adamowicz L, Rode W. 1993. Structure and conformation of N4-hydroxycytosine and N4-hydroxy-5-fluorocytosine. A theoretical ab initio study. Biochim Biophys Acta 1173:39–48. https://doi.org/10.1016/0167-4781(93)90240-E.
42. Crotty S, Cameron CE, Andino R. 2001. RNA virus error catastrophe: direct molecular test by using ribavirin. Proc Natl Acad Sci U S A 98:6895–6900. https://doi.org/10.1073/pnas.111085598.
43. Stuyver LJ, Whitaker T, McBrayer TR, Hernandez-Santiago BI, Lostia S, Tharnish PM, Ramesh M, Chu CK, Jordan R, Shi J, Rachakonda S, Watanabe KA, Otto MJ, Schinazi RF. 2003. Ribonucleoside analogue that blocks replication of bovine viral diarrhea and hepatitis C viruses in culture. Antimicrob Agents Chemother 47:244–254. https://doi.org/10.1128/AAC.47.1.244-254.2003.
44. Moore ML, Chi MH, Luongo C, Lukacs NW, Polosukhin VV, Huckabee MM, Newcomb DC, Buchholz UJ, Crowe JE, Jr, Goleniewska K, Williams JV, Collins PL, Peebles RS, Jr. 2009. A chimeric A2 strain of respiratory syncytial virus (RSV) with the fusion protein of RSV strain line 19 exhibits enhanced viral load, mucus, and airway dysfunction. J Virol 83:4185–4194. https://doi.org/10.1128/JVI.01853-08.
45. Chockalingam AK, Hamed S, Goodwin DG, Rosenzweig BA, Pang E, Boyne MT, II, Patel V. 2016. The effect of oseltamivir on the disease progression of lethal influenza A virus infection: plasma cytokine and miRNA responses in a mouse model. Dis Markers 2016:9296457. https://doi.org/10.1155/2016/9296457.
46. Yen HL, Aldridge JR, Boon AC, Ilyushina NA, Salomon R, Hulse-Post DJ, Marjuki H, Franks J, Boltz DA, Bush D, Lipatov AS, Webby RJ, Rehg JE, Webster RG. 2009. Changes in H5N1 influenza virus hemagglutinin receptor binding domain affect systemic spread. Proc Natl Acad Sci U S A 106:286–291. https://doi.org/10.1073/pnas.0811052106.
47. Bouvier NM, Lowen AC. 2010. Animal models for influenza virus pathogenesis and transmission. Viruses 2:1530–1563. https://doi.org/10.3390/v20801530.
48. Lowen AC, Mubareka S, Tumpey TM, Garcia-Sastre A, Palese P. 2006. The guinea pig as a transmission model for human influenza viruses. Proc Natl Acad Sci U S A 103:9988–9992. https://doi.org/10.1073/pnas.0604157103.
49. Baranovich T, Wong SS, Armstrong J, Marjuki H, Webby RJ, Webster RG, Govorkova EA. 2013. T-705 (favipiravir) induces lethal mutagenesis in influenza A H1N1 viruses in vitro. J Virol 87:3741–3751. https://doi.org/10.1128/JVI.02346-12.
50. Crotty S, Maag D, Arnold JJ, Zhong W, Lau JY, Hong Z, Andino R, Cameron CE. 2000. The broad-spectrum antiviral ribonucleoside ribavirin is an RNA virus mutagen. Nat Med 6:1375–1379. https://doi.org/10.1038/82191.
51. Banks GR, Brown DM, Streeter DG, Grossman L. 1971. Mutagenic analogues of cytosine: RNA polymerase template and substrate studies. J Mol Biol 60:425–439. https://doi.org/10.1016/0022-2836(71)90179-3.
52. Budowsky EI, Sverdlov ED, Monastyrskaya GS. 1972. New method of selective and rapid modification of the cytidine residues. FEBS Lett 25:201–204. https://doi.org/10.1016/0014-5793(72)80485-X.
53. Traut TW. 1994. Physiological concentrations of purines and pyrimidines. Mol Cell Biochem 140:1–22. https://doi.org/10.1007/BF00928361.
54. Lauring AS, Frydman J, Andino R. 2013. The role of mutational robustness in RNA virus evolution. Nat Rev Microbiol 11:327–336. https://doi.org/10.1038/nrmicro3003.
55. Crotty S, Andino R. 2002. Implications of high RNA virus mutation rates: lethal mutagenesis and the antiviral drug ribavirin. Microbes Infect 4:1301–1307. https://doi.org/10.1016/S1286-4579(02)00008-4.
56. Pauly MD, Lauring AS. 2015. Effective lethal mutagenesis of influenza virus by three nucleoside analogs. J Virol 89:3584–3597. https://doi.org/10.1128/JVI.03483-14.
57. Jin Z, Smith LK, Rajwanshi VK, Kim B, Deval J. 2013. The ambiguous base-pairing and high substrate efficiency of T-705 (favipiravir) ribofuranosyl 5′-triphosphate towards influenza A virus polymerase. PLoS One 8:e68347. https://doi.org/10.1371/journal.pone.0068347.
58. Graci JD, Cameron CE. 2006. Mechanisms of action of ribavirin against distinct viruses. Rev Med Virol 16:37–48. https://doi.org/10.1002/rmv.483.
59. Salganik RI, Vasjunina EA, Poslovina AS, Andreeva IS. 1973. Mutagenic action of N4-hydroxycytidine on Escherichia coli B cyt. Mutat Res 20:1–5. https://doi.org/10.1016/0027-5107(73)90091-2.
60. Jakobs HH, Froriep D, Havemeyer A, Mendel RR, Bittner F, Clement B. 2014. The mitochondrial amidoxime reducing component (mARC): involvement in metabolic reduction of N-oxides, oximes and N-hydroxyamidinohydrazones. ChemMedChem 9:2381–2387. https://doi.org/10.1002/cmdc.201402127.
61. Janion C. 1984. Some problems of mutagenesis induced by base analogues. Acta Biochim Pol 31:183–192.
62. Yan D, Lee S, Thakkar VD, Luo M, Moore ML, Plemper RK. 2014. Cross-resistance mechanism of respiratory syncytial virus against structurally diverse entry inhibitors. Proc Natl Acad Sci U S A 111:E3441–E3449. https://doi.org/10.1073/pnas.1405198111.
63. Krumm SA, Yan D, Hovingh ES, Evers TJ, Enkirch T, Reddy GP, Sun A, Saindane MT, Arrendale RF, Painter G, Liotta DC, Natchus MG, von Messling V, Plemper RK. 2014. An orally available, small-molecule polymerase inhibitor shows efficacy against a lethal morbillivirus infection in a large animal model. Sci Transl Med 6:232ra52. https://doi.org/10.1126/scitranslmed.3008517.
64. CDC. 2006. High levels of adamantane resistance among influenza A (H3N2) viruses and interim guidelines for use of antiviral agents—United States, 2005-06 influenza season. JAMA 295:881–882. https://doi.org/10.1001/jama.295.8.881.
65. Okomo-Adhiambo M, Nguyen HT, Abd Elal A, Sleeman K, Fry AM, Gubareva LV. 2014. Drug susceptibility surveillance of influenza viruses circulating in the United States in 2011-2012: application of the WHO antiviral working group criteria. Influenza Other Respir Viruses 8:258–265. https://doi.org/10.1111/irv.12215.
66. Marjuki H, Mishin VP, Chesnokov AP, Jones J, De La Cruz JA, Sleeman K, Tamura D, Nguyen HT, Wu HS, Chang FY, Liu MT, Fry AM, Cox NJ, Villanueva JM, Davis CT, Gubareva LV. 14 August 2014. Characterization of drug-resistant influenza A(H7N9) variants isolated from an oseltamivir-treated patient in Taiwan. J Infect Dis https://doi.org/10.1093/infdis/jiu447.
67. Nguyen HT, Fry AM, Gubareva LV. 2012. Neuraminidase inhibitor resistance in influenza viruses and laboratory testing methods. Antivir Ther 17:159–173. https://doi.org/10.3851/IMP2067.
68. McKimm-Breschkin JL, Williams J, Barrett S, Jachno K, McDonald M, Mohr PG, Saito T, Tashiro M. 2013. Reduced susceptibility to all neuraminidase inhibitors of influenza H1N1 viruses with haemagglutinin mutations and mutations in non-conserved residues of the neuraminidase. J Antimicrob Chemother 68:2210–2221. https://doi.org/10.1093/jac/dkt205.
69. McKimm-Breschkin JL. 2013. Influenza neuraminidase inhibitors: antiviral action and mechanisms of resistance. Influenza Other Respir Viruses 7(Suppl 1):S25–S36. https://doi.org/10.1111/irv.12047.
70. Stokes KL, Chi MH, Sakamoto K, Newcomb DC, Currier MG, Huckabee MM, Lee S, Goleniewska K, Pretto C, Williams JV, Hotard A, Sherrill TP, Peebles RS, Jr, Moore ML. 2011. Differential pathogenesis of respiratory syncytial virus clinical isolates in BALB/c mice. J Virol 85:5782–5793. https://doi.org/10.1128/JVI.01693-10.
71. Peebles RS, Jr, Graham BS. 2005. Pathogenesis of respiratory syncytial virus infection in the murine model. Proc Am Thorac Soc 2:110–115. https://doi.org/10.1513/pats.200501-002AW.
72. Belser JA, Wadford DA, Pappas C, Gustin KM, Maines TR, Pearce MB, Zeng H, Swayne DE, Pantin-Jackwood M, Katz JM, Tumpey TM. 2010. Patho-

genesis of pandemic influenza A (H1N1) and triple-reassortant swine influenza A (H1) viruses in mice. J Virol 84:4194–4203. https://doi.org/10.1128/JVI.02742-09.
73. Belser JA, Lu X, Maines TR, Smith C, Li Y, Donis RO, Katz JM, Tumpey TM. 2007. Pathogenesis of avian influenza (H7) virus infection in mice and ferrets: enhanced virulence of Eurasian H7N7 viruses isolated from humans. J Virol 81:11139–11147. https://doi.org/10.1128/JVI.01235-07.
74. Yang YT, Evans CA. 1961. Hypothermia in mice due to influenza virus infection. Proc Soc Exp Biol Med 108:776–780. https://doi.org/10.3181/00379727-108-27064.
75. Sudo K, Watanabe W, Mori S, Konno K, Shigeta S, Yokota T. 1999. Mouse model of respiratory syncytial virus infection to evaluate antiviral activity in vivo. Antivir Chem Chemother 10:135–139. https://doi.org/10.1177/095632029901000305.
76. Mok CK, Lee HH, Chan MC, Sia SF, Lestra M, Nicholls JM, Zhu H, Guan Y, Peiris JM. 2013. Pathogenicity of the novel A/H7N9 influenza virus in mice. mBio 4:e00362-13. https://doi.org/10.1128/mBio.00362-13.
77. Kang YM, Song BM, Lee JS, Kim HS, Seo SH. 2011. Pandemic H1N1 influenza virus causes a stronger inflammatory response than seasonal H1N1 influenza virus in ferrets. Arch Virol 156:759–767. https://doi.org/10.1007/s00705-010-0914-7.
78. Hayden FG, Fritz R, Lobo MC, Alvord W, Strober W, Straus SE. 1998. Local and systemic cytokine responses during experimental human influenza A virus infection. Relation to symptom formation and host defense. J Clin Invest 101:643–649. https://doi.org/10.1172/JCI1355.
79. Paquette SG, Banner D, Zhao Z, Fang Y, Huang SS, Leomicronn AJ, Ng DC, Almansa R, Martin-Loeches I, Ramirez P, Socias L, Loza A, Blanco J, Sansonetti P, Rello J, Andaluz D, Shum B, Rubino S, de Lejarazu RO, Tran D, Delogu G, Fadda G, Krajden S, Rubin BB, Bermejo-Martin JF, Kelvin AA, Kelvin DJ. 2012. Interleukin-6 is a potential biomarker for severe pandemic H1N1 influenza A infection. PLoS One 7:e38214. https://doi.org/10.1371/journal.pone.0038214.
80. Killian ML. 2008. Hemagglutination assay for the avian influenza virus. Methods Mol Biol 436:47–52. https://doi.org/10.1007/978-1-59745-279-3_7.
81. National Research Council. 2011. Guide for the care and use of laboratory animals, 8th ed. National Academies Press, Washington, DC.
82. Razinkov V, Huntley C, Ellestad G, Krishnamurthy G. 2002. RSV entry inhibitors block F-protein mediated fusion with model membranes. Antiviral Res 55:189–200. https://doi.org/10.1016/S0166-3542(02)00050-5.
83. Hampp C, Kauf TL, Saidi AS, Winterstein AG. 2012. Methodological concerns regarding cost-effectiveness analysis of palivizumab in Florida Medicaid—reply. Arch Pediatr Adolesc Med 166:968–970. https://doi.org/10.1001/archpediatrics.2012.1594.